Supporting Information

Metal-Silicon Triple Bonds: Access to $[Si(\eta^5\text{-}C_5Me_5)]^+$ from SiX_2(NHC) and Its Conversion to the Silylidyne Complex $[Tp^{Me}(CO)_2MoSi(\eta^3\text{-}C_5Me_5)]$ (Tp^{Me} = κ^3-*N,N',N''*-Hydridotris(3,5-dimethyl-1-pyrazolyl)borate)

Priyabrata Ghana,[a] Marius I. Arz,[b] Gregor Schnakenburg,[a] Martin Straßmann[a] and Alexander C. Filippou[a,*]

[a]: Institut für Anorganische Chemie, Rheinische Friedrich-Wilhelms-Universität Bonn, Gerhard-Domagk-Straße 1, D-53121 Bonn, Germany
E-mail: filippou@uni-bonn.de

[b]: University of Bristol, School of Chemistry, Cantock's Close, Bristol, BS8 1TS

Content

1. Experimental Section – General Part S2

2. Syntheses and analytical data of the compounds S4

2.1 Synthesis of $SiCp^*_2$ ($Cp^* = C_5Me_5$) (**1**) S4

2.1.1 Synthesis of $SiCp^*_2$ (**1**) from $SiCl_2$(Idipp) S4

2.1.2 Synthesis of $SiCp^*_2$ (**1**) from other SiX_2(NHC) compounds S7

2.2 Synthesis of $[Si(\eta^5\text{-}Cp^*)][B(C_6F_5)_4]$ (**2**) S7

2.3 Synthesis of $[Tp^{Me}(CO)_2MoSi(\eta^3\text{-}Cp^*)]$ (**3**) S11

3. Crystal structure determination S16

4. Electronic structure calculations S17

4.1 Comparison of selected bonding parameters of **3** and $\mathbf{3_{calc}}$ S18

4.2 Selected Kohn-Sham orbitals of $\mathbf{3_{calc}}$ S19

4.3 Selected results of the NBO and NRT analyses of $\mathbf{3_{calc}}$ S20

4.4 Calculation of the PES of the haptotropic shift of **3** S22

4.5 Calculated structure and NBO and NRT analyses of $[Si(\eta^5\text{-}Cp^*)]^+$ S24

4.6 Calculated structure and NBO and NRT analyses of $[Cp^*(CO)_2FeSi(\eta^3\text{-}Cp^*)]$ S24

1. Experimental Section – General Part

All experiments were carried out under an atmosphere of argon using Schlenk or glove box techniques. Argon was commercially received with a purity of ≥99.999 % and passed through a gas purification system composed of two consecutive columns to remove traces of oxygen and water. The first column was filled with BTS copper catalyst R3-11G from BASF and heated at ca. 80 °C and the second column with 4 Å molecular sieves. The glassware was dried in an oven at approximately 110 °C and baked under vacuum prior to use.

The solvents were refluxed several days over the respective drying reagent (*n*-pentane, *n*-hexane: sodium wire / benzophenone / tetraglyme (0.5 vol%); toluene: sodium wire; diethyl ether, tetrahydrofuran (THF): sodium wire / benzophenone; fluorobenzene: CaH_2; dichloromethane: Sicapent® followed by Na/Pb alloy), purged several times during reflux with argon, distilled off under argon and degassed by freeze-pump-thaw cycles. All solvents were stored in the glove box.

C, H, N elemental analyses were carried out in triplicate for each sample on an Elementar Vario Micro elemental analyser. The C, H, N values did not differ by more than ±0.3 %. The mean C, H, N values are given below for each compound.

The thermal behavior of the starting materials $[Tp^{Me}Mo(CO)_2(PMe_3)Cl]$, $Na[Tp^{Me}Mo(CO)_2(PMe_3)]$, of compound **2** and of the silylidyne complex **3** was studied in triplicate in vacuum-sealed capillary tubes using a Büchi B545 melting point apparatus. The first samples were heated with a gradient of 5 K min^{-1} for a rough determination of the temperature of melting or starting decomposition. Heating of the second and third sample was then repeated with a gradient of 2 K min^{-1}, starting 20 K below the temperature of melting or starting decomposition determined in the first experiment. Decomposition of $[Tp^{Me}Mo(CO)_2(PMe_3)Cl]$, $Na[Tp^{Me}Mo(CO)_2(PMe_3)]$ and **3** was concluded by ATR-IR spectra of the heated samples, and melting of **2** without decomposition was confirmed by a ^1H NMR spectrum of the heated sample.

ATR-IR spectra in the solid state were recorded in the spectral range of 4000 – 400 cm^{-1} at room temperature on a Bruker Alpha FT-IR spectrometer in a glove box using a platinum single reflection diamond ATR module. IR spectra in solution were recorded at room temperature on a Nicolet 380 FTIR spectrometer in the spectral range of 4000 – 600 cm^{-1} using a cell of NaCl windows, which were separated by a Teflon spacer with a thickness of 0.20 mm. The solution IR spectra were background corrected for the solvent absorptions. The following abbreviations were used for the intensities of the absorption bands: vs = very strong, s = strong, m = medium, w = weak, vw = very weak.

The NMR spectra were recorded on a Bruker Avance DMX-300, DPX-400 or DMX-500 MHz spectrometer in dry deoxygenated benzene-d_6, dichloromethane-d_2 or THF-d_8. The deuterated solvents were trap-to-trap condensed after stirring over sodium powder (benzene-

d_6, THF-d_8) or CaH_2 (dichloromethane-d_2) and stored over molecular sieves (4 Å). The ^{1}H and ^{13}C{^{1}H} NMR spectra were calibrated against the residual proton and natural abundance ^{13}C resonances of the deuterated solvent relative to tetramethylsilane (benzene-d_6: δ_H = 7.15 ppm and δ_C = 128.0 ppm; dichloromethane-d_2: δ_H = 5.32 ppm and δ_C = 53.8 ppm; THF-d_8: δ_H = 1.73 ppm and δ_C = 25.3 ppm). The ^{29}Si and ^{31}P NMR spectra were calibrated against external pure tetramethylsilane and a 85 % aqueous H_3PO_4 solution, respectively. For this purpose the standards were sealed in capillaries and measured in vacuum-sealed 5 mm NMR tubes containing the respective deuterated solvent to obtain the SR value of each solvent. The following abbreviations were used for the multiplicities and forms of the NMR signals: s: singlet, d: doublet, t: triplet, sept: septet, br: broad. The ^{1}H and ^{13}C NMR signals of **3** were assigned by a combination of HMQC, HMBC and DEPT experiments. In addition, selective 1D transient (DPFGSE) NOE experiments were carried out to assign the C^3- and C^5-bonded methyl protons of the Tp^{Me} ligand. These experiments allowed in combination with the HMQC and HMBC experiments to assign unequivocally the C^3 and C^5 resonances of the 3,5-dimethylpyrazolyl groups. The label pz_A was used to denote the two symmetry-equivalent (enantiotopic) 3,5-dimethylpyrazolyl groups of the Tp^{Me} ligand and the label pz_B for the third (diastereotopic) 3,5-dimethylpyrazolyl arm of the Tp^{Me} ligand lying in the symmetry plane of the overall pseudo-C_s symmetric complex **3**.

The compounds $SiCl_2$(Idipp)[S1] (Idipp = $C[N(C_6H_3\text{-}2,6\text{-}i\text{Pr}_2)CH]_2$), KCp* (Cp* = C_5Me_5)[S2] and $[H(Et_2O)_2][B(C_6F_5)_4]$[S3] were prepared following the literature procedures. The metalate $Na[Tp^{Me}Mo(CO)_2(PMe_3)]$ (Tp^{Me} = κ^3-N,N',N''-hydridotris(3,5-dimethyl-1-pyrazolyl)borate) was obtained in two steps starting from $[Tp^{Me}Mo(CO)_2Cl]$.[S4] In the first step, $[Tp^{Me}Mo(CO)_2Cl]$ was treated with one equivalent of PMe_3 in CH_2Cl_2 at −30 °C to afford $[Tp^{Me}Mo(CO)_2(PMe_3)Cl]$ as a bright yellow solid in 92 % yield.[S5] Subsequent two-electron reduction of $[Tp^{Me}Mo(CO)_2(PMe_3)Cl]$ with two equivalents of a 0.38 M sodium naphthalenide

[S1] Ghadwal, R. S.; Roesky, H. W.; Merkel, S.; Henn, J.; Stalke, D.; *Angew. Chem. Int. Ed.* **2009**, *48*, 5683; *Angew. Chem.* **2009**, *121*, 5793.

[S2] Behrens, U.; Dinnebier, R. E.; Neander, S.; Olbrich, F. *Organometallics* **2008**, *27*, 5398.

[S3] Jutzi, P.; Müller, C.; Stammler, A.; Stammler, H.-G. *Organometallics* **2000**, *19*, 1442.

[S4] Saleh, A. A.; Pleune, B.; Fettinger, J. C.; Poli, R. *Polyhedron* **1997**, *16*, 1391.

[S5] Selected analytical data of $[Tp^{Me}Mo(CO)_2(PMe_3)Cl]$: Elemental analysis calcd. (%) for $C_{20}H_{31}BClMoN_6O_2P$ (560.68 g mol^{-1}): C 42.84, H 5.57, N 14.99; found: C 42.55, H 5.71, N 15.52 %. The bright yellow solid slowly turns brown above 184 °C and decomposes upon melting at 221–222 °C to give a black oily mass. IR (CH_2Cl_2, 298 K, cm^{-1}): ν = 1940 (s) and 1841 (vs) [ν(CO)], 1546 (m) [ν(C-C-N)$_{pz}$]; IR (THF, 298 K, cm^{-1}): ν = 1936 (s) and 1840 (vs) [ν(CO)], 1547 (m) [ν(C-C-N)$_{pz}$]. ^{1}H NMR (300.1 MHz, dichloromethane-d_2, 298 K, ppm): δ = 2.03 (s, 3H, 1 × C^3-*Me*, pz_B), 2.10 (d, ^2J(P,H) = 10.5 Hz, 9H, P*Me*$_3$), 2.33 (s, 6H, 2 × C^3-*Me*, pz_A), 2.43 (s, 9H, 2 × C^5-*Me* (pz_A) and 1 × C^5-*Me* (pz_B)), 4.78 (br, 1H, B*H*; this signal appears as a very broad hump over the base line in a strongly enlarged version of the spectrum), 5.90 (s, 3H, 3 × C^4-*H*, pz_A and pz_B). ^{31}P{^{1}H} NMR (121.5 MHz, dichloromethane-d_2, 298 K, ppm): δ = 33.7 (s).

solution in THF at ambient temperature yielded Na[Tp^{Me}Mo(CO)$_2$(PMe$_3$)], which was isolated as an extremely air-sensitive yellow solid in 95 % yield.[S6]

2. Syntheses and analytical data of the compounds

2.1 Synthesis of SiCp*$_2$ (Cp* = C$_5$Me$_5$) (1)

2.1.1 Synthesis of SiCp*$_2$ (1) from SiCl$_2$(Idipp)

A mixture of slightly yellow SiCl$_2$(Idipp) (1.428 g, 2.93 mmol) and colorless KCp* (1.022 g, 5.86 mmol, 2.0 equiv.) was cooled to −30 °C and 40 mL of precooled (−60 °C) diethyl ether were added rapidly using a 2 mm transfer cannula. The yellowish suspension was stirred for 30 minutes at −30 °C, warmed to room temperature and further stirred at room temperature for 1 h. The solvent was removed under vacuum and the resulting pale yellow solid was dried for 1 h under vacuum at room temperature. A ^{1}H NMR spectrum of the solid in benzene-d_6 revealed a selective and quantitative conversion of the starting materials into **1** and Idipp.[S7] The solid was cooled to −40 °C, 15 mL of precooled (−60 °C) *n*-hexane were added, and the suspension was stirred for 5 minutes at −60 °C. It was filtered at −60 °C and the extraction was repeated twice with 2 × 15 mL of *n*-hexane. A colorless residue (1.607 g after drying)[S8] and a pale yellow filtrate were obtained. The filtrate was evaporated to dryness under vacuum at room temperature, and the obtained colorless solid was further dried under vacuum for 1 h at room temperature. Yield: 686 mg (2.30 mmol, 78 % from SiCl$_2$(Idipp)).[S9]

[S6] Selected analytical data of Na[Tp^{Me}Mo(CO)$_2$(PMe$_3$)]: Melting point: The yellow solid slowly turns gray above 271 °C and decomposes upon melting at 288 °C to give a black liquid. IR (THF, 298 K, cm^{-1}): ν = 1766 (m), 1726 (vs), 1644 (m), 1620 (s) and 1596 (s) [ν(CO)], 1546 (m) [ν(C-C-N)$_{pz}$]. IR (MeCN, 298 K, cm^{-1}): ν = 1755 (vs) and 1663 (vs) [ν(CO)], 1545 (m) [ν(C-C-N)$_{pz}$]. ^{1}H NMR (300.1 MHz, THF-d_8, 298 K, ppm): δ = 1.27 (d, ^2J(P,H) = 5.8 Hz, 9H, P*Me*$_3$), 2.22 (s, 3H, 1 × C^5-*Me*, pz$_B$), 2.34 (s, 6H, 2 × C^5-*Me*, pz$_A$), 2.43 (s, 3H, 1 × C^3-*Me*, pz$_B$), 2.53 (s, 6H, 2 × C^3-*Me*, pz$_A$), 4.6 (br, 1H, B*H*; this signal appears as a very broad hump over the base line in a strongly enlarged version of the spectrum), 5.47 (s, 1H, 1 × C^4-*H*, pz$_B$), 5.63 (s, 2H, 2 × C^4-*H*, pz$_A$). ^{31}P{^{1}H} NMR (121.5 MHz, THF-d_8, 298 K, ppm): δ = 15.8 (s).

[S7] ^{1}H NMR spectroscopic data of Idipp (400.1 MHz, benzene-d_6 298 K, ppm): δ = 1.18 (d, ^3J(H,H) = 6.7 Hz, 12H, 2 × C^{2,6}-CH*Me*$_A$Me$_B$), 1.28 (d, ^3J(H,H) = 6.7 Hz, 12H, 2 × C^{2,6}-CHMe$_A$*Me*$_B$), 2.96 (sept, ^3J(H,H) = 6.7 Hz, 4H, 2 × C^{2,6}-C*H*Me$_A$Me$_B$), 6.61 (s, 2H, C^{4,5}-*H*), 7.18 (d, ^3J(H,H) = 7.8 Hz, 4H, 2 × C^{3,5}-*H*, C$_6$H$_3$), 7.28 (t, ^3J(H,H) = 7.8 Hz, 2H, 2 × C^4-*H*, C$_6$H$_3$).

[S8] A ^{1}H NMR spectrum of the residue after extraction showed only a very small amount of **1** indicating an almost quantitative extraction of the product.

[S9] The reaction was repeated several times and in few cases the isolated product was contaminated with a tiny amount of Cp*H or Idipp. In this case, the product was purified by fractional sublimation as described in 2.1.2. ^{1}H NMR spectroscopic data of Cp*H (300.1 MHz, benzene-d_6, 298 K, ppm): δ = 0.98 (d, ^3J(H,H) = 7.6 Hz, 3H, C^5-(H)*Me*), 1.73, 1.79 (each s, each 6H, C^{1,4}-*Me* + C^{2,3}-*Me*), 2.41 (q, ^3J(H,H) = 7.6 Hz, 1H, C^5-(*H*)Me); (see: Filippou, A. C.; Schnakenburg, G.; Philippopoulos, A. I.; Weidemann, N. *Angew. Chem. Int. Ed.* **2005**, *44*, 5979; *Angew. Chem.* **2005**, *117*, 6133).

Elemental analysis calcd (%) for $C_{20}H_{30}Si$ (298.54): C 80.46, H 10.13; found: C 80.05, H 10.03 %.

^{1}H NMR (*Figure S1*, 300.1 MHz, benzene-d_6, 298 K, ppm): δ = 1.89 (s, 30H, 2 × C_5Me_5).

^{13}C{^{1}H} NMR (*Figure S2*, 125.8 MHz, benzene-d_6, 298 K, ppm): δ = 10.4 (s, 10C, 2 × C_5Me_5), 119.1 (s, 10C, 2 × C_5Me_5).

^{29}Si{^{1}H} NMR (*Figure S3*, 99.33 MHz, benzene-d_6, 298 K, ppm): δ = −392.9 (s).[S10]

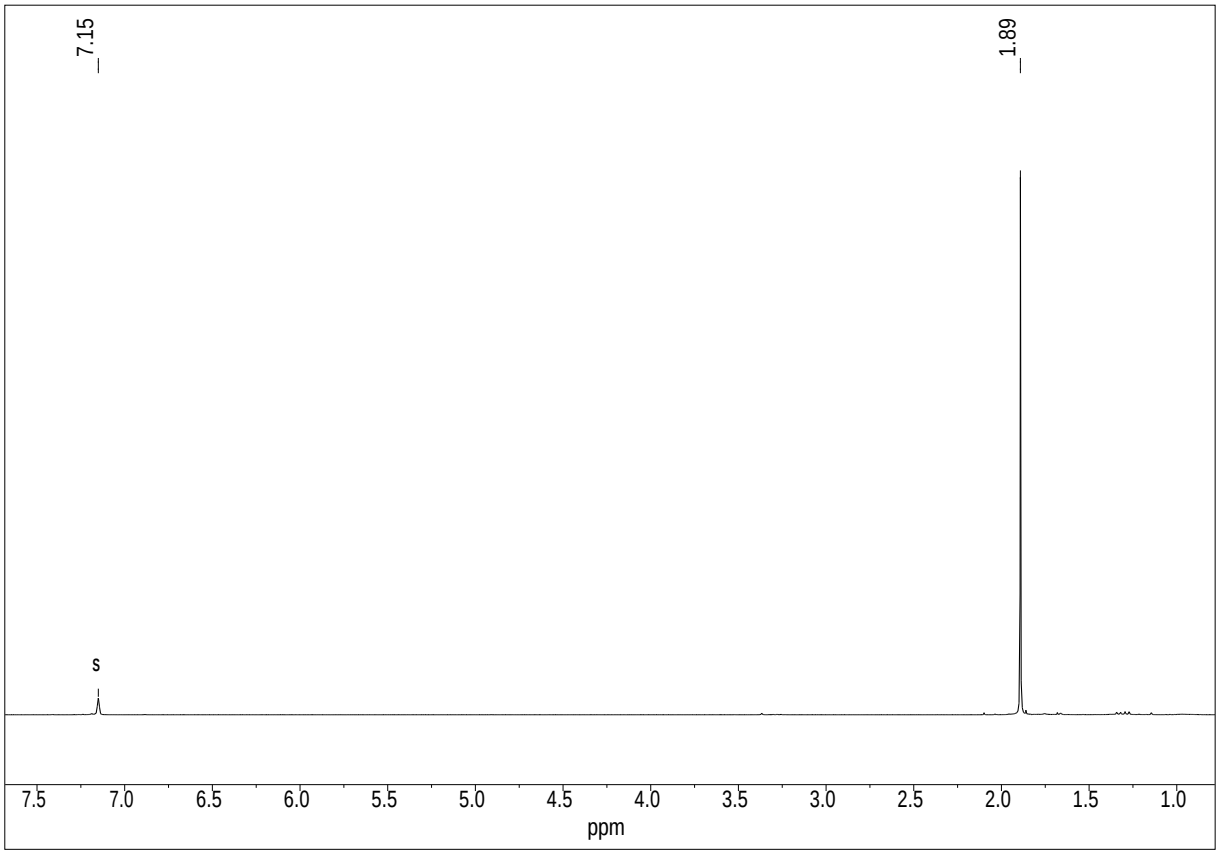

Figure S1. ^{1}H NMR (300.1 MHz) spectrum of **1** in benzene-d_6 at 298 K; the residual proton signal of the deuterated solvent is marked with the character S.

[S10] The spectroscopic data compare well with those given in: Jutzi, P.; Holtmann, U.; Kanne, D. Krüger, C.; Blom, R.; Gleiter, R.; Hyla-Kryspin, I. *Chem. Ber.* **1989**, *122*, 1629. Note that an erroneous ^{29}Si NMR signal was reported for **1** (δ = −577 ppm in benzene-d_6) in: Jutzi, P.; Kanne, D.; Krüger, C. *Angew. Chem. Int. Ed.* **1986**, *25*, 164; *Angew. Chem.* **1986**, *98*, 163.

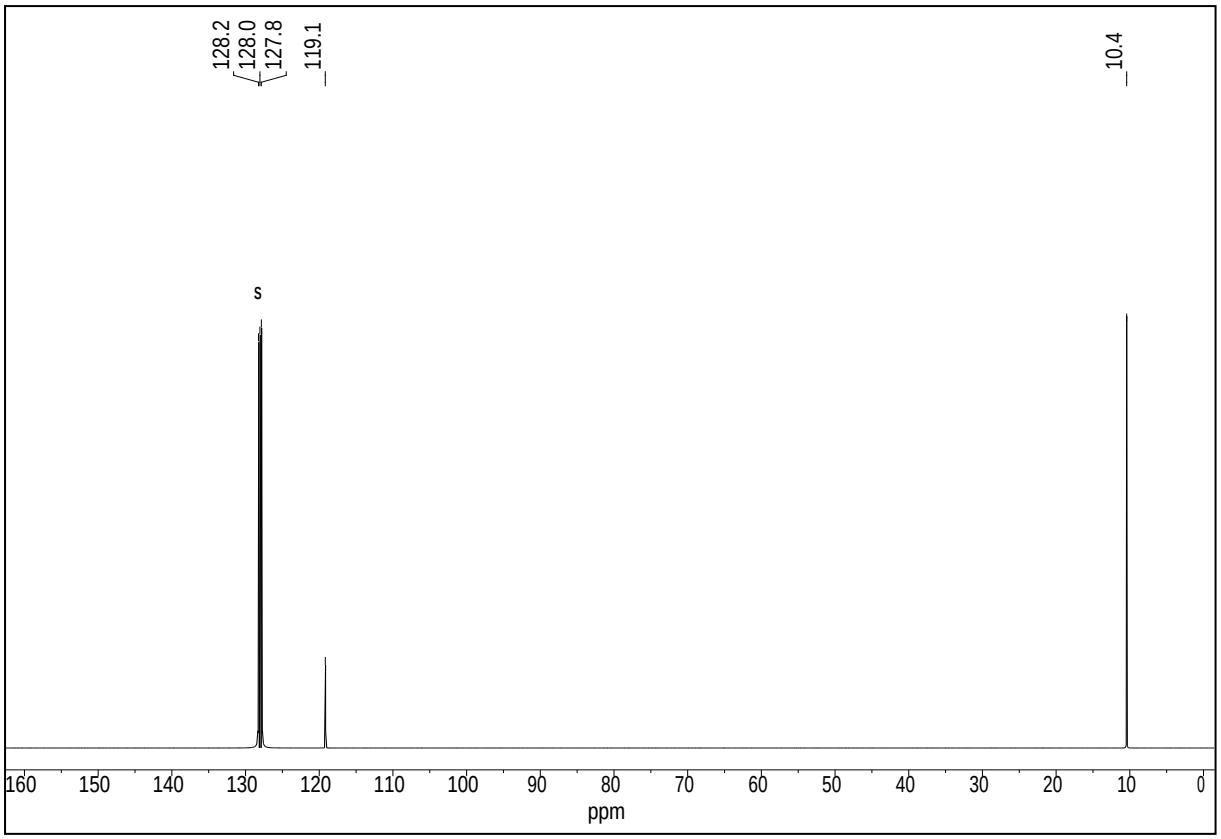

Figure S2. $^{13}C\{^{1}H\}$ NMR (125.8 MHz) spectrum of **1** in benzene-d_6 at 298 K; the signal of the deuterated solvent is marked with the character S.

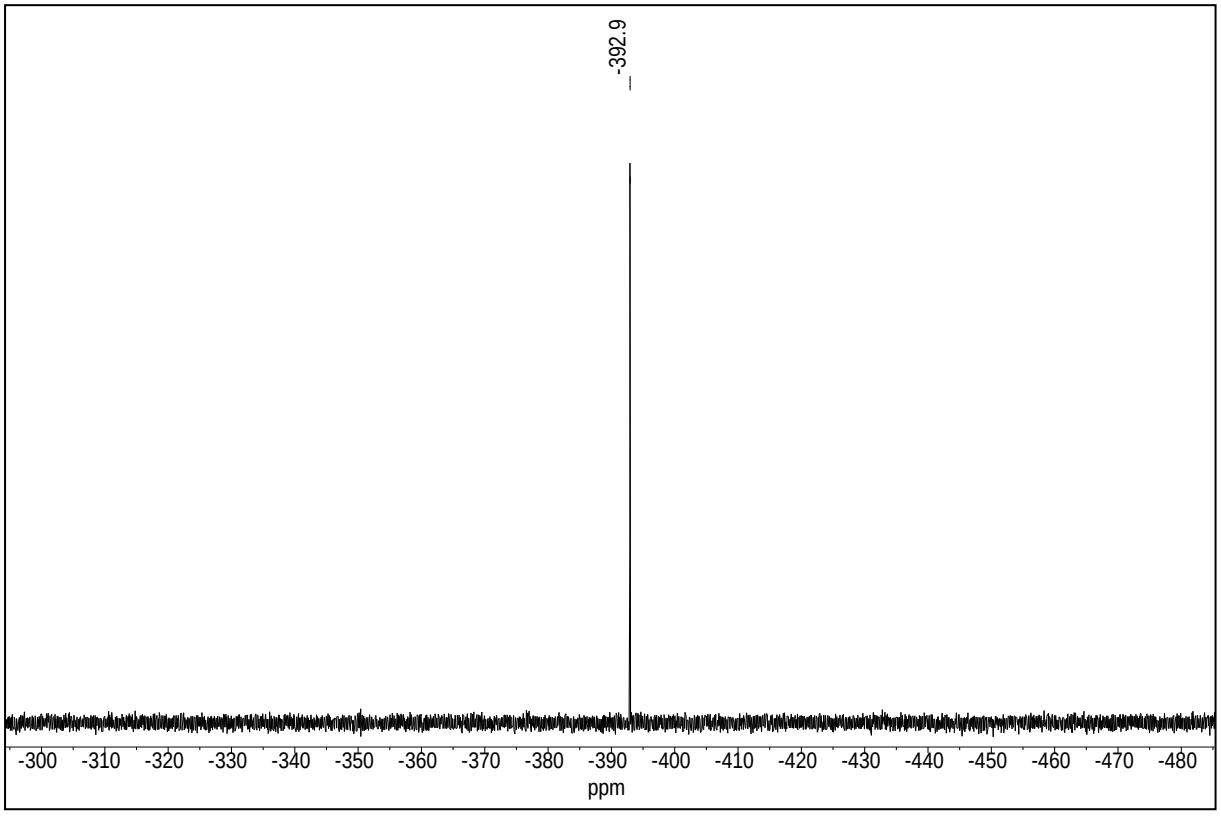

Figure S3. $^{29}Si\{^{1}H\}$ NMR (99.33 MHz) spectrum of **1** in benzene-d_6 at 298 K.

2.1.2 Synthesis of $SiCp^*_2$(1) starting from other SiX_2(NHC) compounds

Additional studies on the synthesis of **1** were carried out starting from other SiX_2(NHC) compounds:

1) Thus, reaction of $SiBr_2$(SIdipp) (SIdipp = $C[N(C_6H_3\text{-}2,6\text{-}i\text{Pr}_2)CH_2]_2$)[S11] with two equivalents of KCp* under identical conditions had the same outcome as that of $SiCl_2$(Idipp) and afforded compound **1** in 73 % yield.
2) In comparison, treatment of $SiBr_2$(Idipp)[S12] or SiI_2(Idipp)[S13] with two equivalents of KCp* in toluene at room temperature led to **1,** but also to bi[(1,2,3,4,5,-pentamethyl)-2,4-cyclopentadienyl] (Cp^*_2)[S14] and Cp*H as evidenced from the ^{1}H NMR spectra of the crude products obtained after evaporation of the solvent. Furthermore, trace amounts of the Si(0) compound $Si_2(Idipp)_2$[S15] and the Si(I) compounds $Si_2Br_2(Idipp)_2$ and $Si_2I_2(Idipp)_2$[S16] were detected in the ^{1}H NMR spectra of the crude products. Purification of **1** was carried out by extraction with *n*-hexane at low temperature and subsequent fractional sublimation ($5 \cdot 10^{-2}$ mbar) as described in the following: Cp*H deposited first at 80 °C – 90 °C (heating bath temperature), and was removed by cleaning the cooling finger with a paper towel, followed by sublimation of the pure product **1** at 105 – 115 °C (heating bath temperature). Thereby, Idipp and Cp*H as well as the Si(0) compound $Si_2(Idipp)_2$ and the Si(I) compound $Si_2X_2(Idipp)_2$ (X = Br, I) could be removed, however the sublimed **1** contained still some Cp^*_2.
3) Similarly, the reaction of SiI_2(Idipp) with two equivalents of KCp* in diethyl ether at −30 °C or room temperature led also to some Cp^*_2 and Cp*H. However, these byproducts were formed to a smaller extent compared to the reaction in toluene under identical conditions.

2.2 Synthesis of $[Si(\eta^5\text{-}Cp^*)][B(C_6F_5)_4]$ (2)

A colourless solution of $[H(Et_2O)_2][B(C_6F_5)_4]$ (2.10 g, 2.54 mmol, 1.0 equiv.) in 8 mL of fluorobenzene was added dropwise via a syringe to a pale yellow solution of compound **1**

[S11] Filippou, A. C.; Chernov, O.; Schnakenburg, G. *Chem. Eur. J.* **2011**, *17*, 13574.

[S12] Filippou, A. C.; Chernov, O.; Schnakenburg, G. *Angew. Chem. Int. Ed.* **2009**, *48*, 5687; *Angew. Chem.* **2009**, *121*, 5797.

[S13] Filippou, A. C.; Lebedev, Y. N.; Chernov, O.; Straßmann, M.; Schnakenburg, G. *Angew. Chem. Int. Ed.* **2013**, *52*, 6974; *Angew. Chem.* **2013**, *125*, 7112.

[S14] Spectroscopic data of bi[(1,2,3,4,5,-pentamethyl)-2,4-cyclopentadienyl]: ^{1}H NMR (300.1 MHz, benzene-d_6, 298 K, ppm) δ = 1.14 (s, 6H, $C^{1,1'}$-*Me*), 1.66, 1.76 (each s, each 12H, $C^{2,2',5,5'}$-*Me* + $C^{3,3',4,4'}$-*Me*); (see also: Jutzi, P.; Kohl, F. *J. Organomet. Chem.* **1979**, *164*, 141).

[S15] Wang, Y.; Xie, Y.; Wei, P.; King, R. B.; Schaefer III, H. F.; Schleyer, P. v. R.; Robinson, G. H. *Science* **2008**, *321*, 1069.

[S16] Arz, M. I.; Geiß, D.; Straßmann, M.; Schnakenburg, G.; Filippou, A. C. *Chem. Sci.* **2015**, *6*, 6515.

(0.757 g, 2.54 mmol) in 5 mL of fluorobenzene at ambient temperature. The resulting light orange solution was stirred for 1.5 h at ambient temperature. The solution was concentrated under vacuum to *ca.* 8 mL, and 50 mL of *n*-pentane were added to the solution, leading to precipitation of a light pink powder. The colourless supernatant was filtered off at ambient temperature and the residue dried under vacuum for 3 h at ambient temperature to give a light pink powder (2.13 g). Recrystallization of the light pink solid from a fluorobenzene/*n*-pentane mixture (8 mL/3 mL) at −30 °C for 16 h afforded compound **2** as an extremely air-sensitive, colourless, microcrystalline solid. Yield: 1.83 g (2.17 mmol, 85 %). The colorless solid melts to a pale yellow liquid at 230 – 233 °C. Elemental analysis calcd (%) for $C_{34}H_{15}BF_{20}Si$ (842.35): C 48.48, H 1.79; found: C 48.74, H 1.85 %.

^{1}H NMR (*Figure S4*, 300.1 MHz, dichloromethane-d_2, 298 K, ppm): δ = 2.23 (s, 15H, C_5Me_5).

^{13}C{^{1}H} NMR (*Figure S5*, 75.47 MHz, dichloromethane-d_2, 298 K, ppm): δ = 9.2 (s, 5C, C_5Me_5), 122.9 (s, ^{1}J(Si,C) = 13.2 Hz, 5C, C_5Me_5), 124.5 (br, $\Delta\nu_{1/2}$ = *ca.* 180 Hz, 4C, 4 × C^{1}-B, C_6F_5), 136.7 (dm, ^{1}J(F,C) = 245 Hz, 8C, 4 × $C^{3,5}$-F, C_6F_5), 138.6 (dt, ^{1}J(F,C) = 245 Hz, ^{2}J(F,C) = 14 Hz, 4C, 4 × C^{4}-F, C_6F_5), 148.5 (dm, ^{1}J(F,C) = 240 Hz, 8C, 4 × $C^{2,6}$-F, C_6F_5).

^{29}Si{^{1}H} NMR (*Figure S6*, 99.34 MHz, dichloromethane-d_2, 298 K, ppm): δ = −398.9 (s).

^{19}F{^{1}H} NMR (*Figure S7*, 282.4 MHz, dichloromethane-d_2, 298 K, ppm): δ = −167.5 (m, 8F, 4 × $C^{3,5}$-*F*, C_6F_5), −163.6 (t, ^{3}J(F,F) = 20.4 Hz, 4F, 4 × C^{4}-*F*, C_6F_5), −133.0 (m, 8F, 4 × $C^{2,6}$-*F*, C_6F_5).

^{11}B{^{1}H} NMR (96.30 MHz, dichloromethane-d_2, 298 K, ppm): δ = −16.7 (s, 1B, $B(C_6F_5)_4$).[S17]

[S17] The spectroscopic data compare well with those reported in: Jutzi, P.; Mix, A.; Rummel, B.; Schoeller, W. W.; Neumann, B.; Stammler, H.-G. *Science* **2004**, *305*, 849.

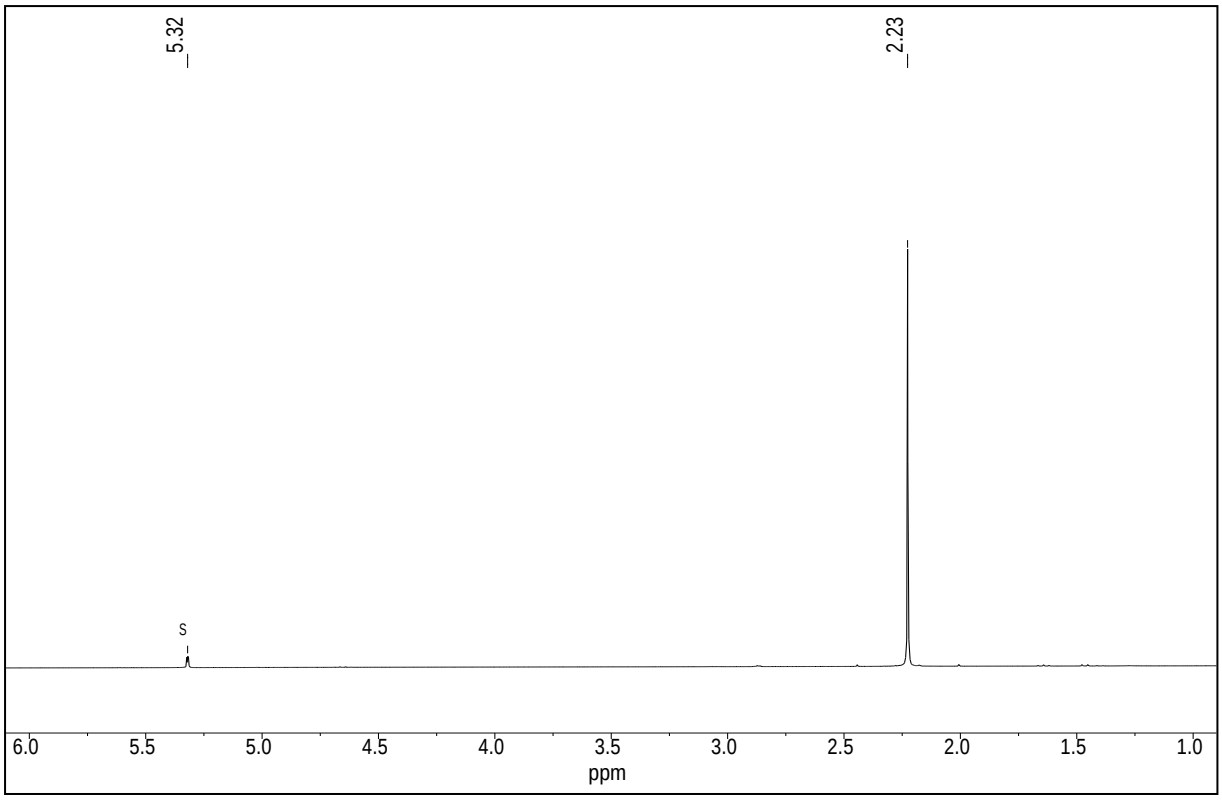

Figure S4. ^{1}H NMR (300.1 MHz) spectrum of **2** in dichloromethane-d_2 at 298 K; the residual proton signal of the deuterated solvent is marked with the character S.

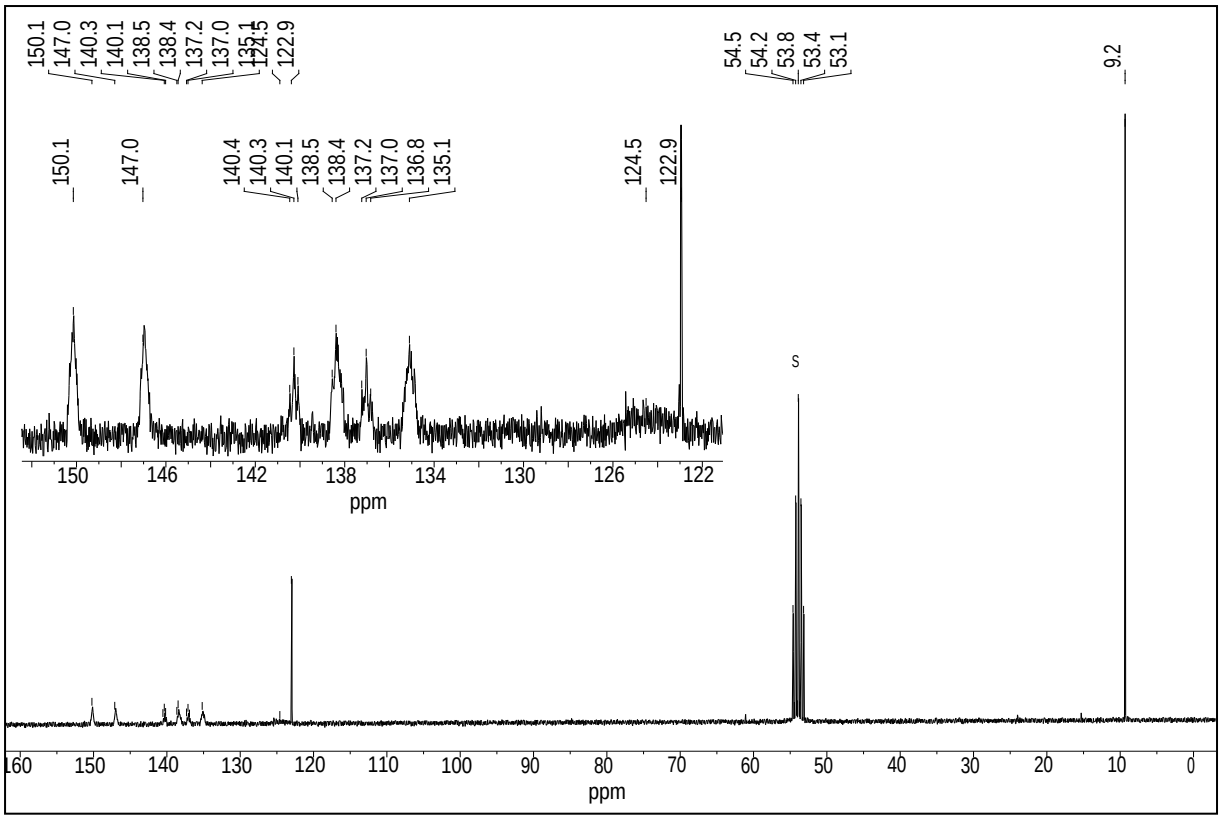

Figure S5. ^{13}C{^{1}H} NMR (75.47 MHz) spectrum of **2** in dichloromethane-d_2 at 298 K; the signal of the deuterated solvent is marked with the character S; an expanded section of the aromatic region of the ^{13}C{^{1}H} NMR spectrum is shown in the inset.

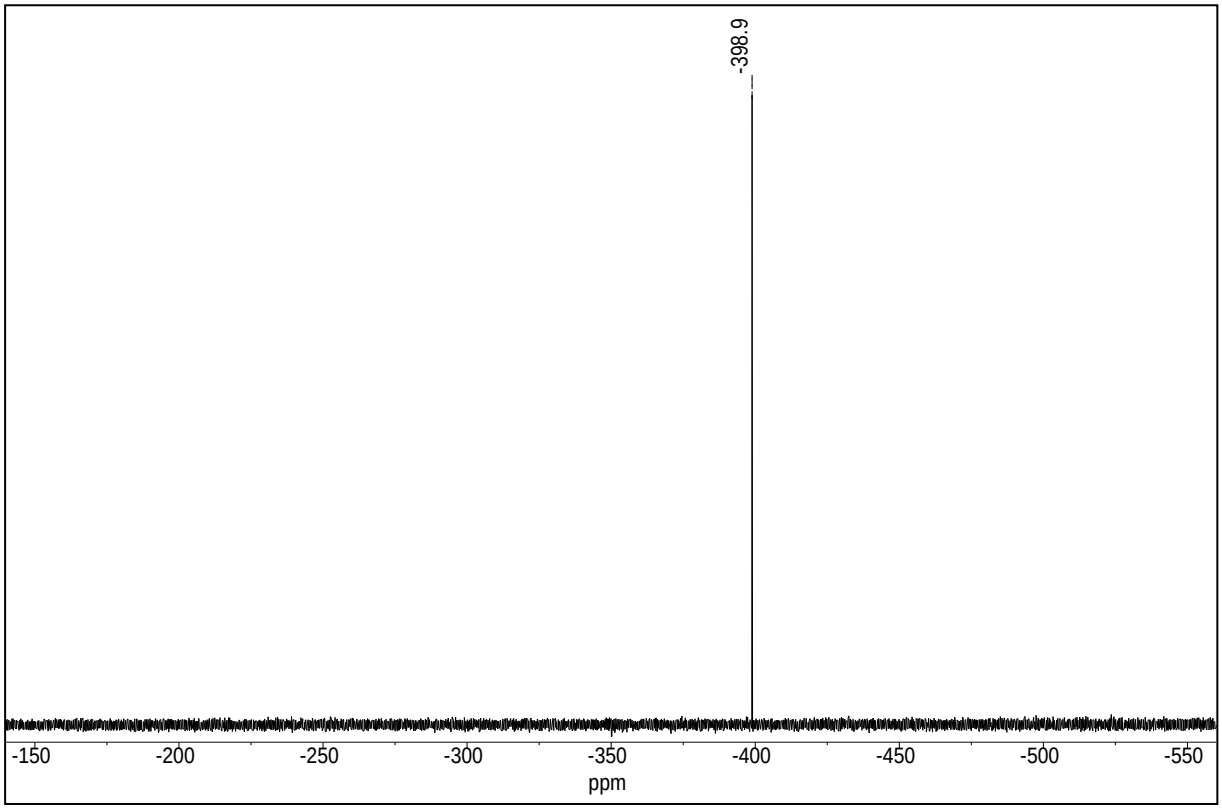

Figure S6. $^{29}Si\{^{1}H\}$ NMR (99.34 MHz) spectrum of **2** in dichloromethane-d_2 at 298 K.

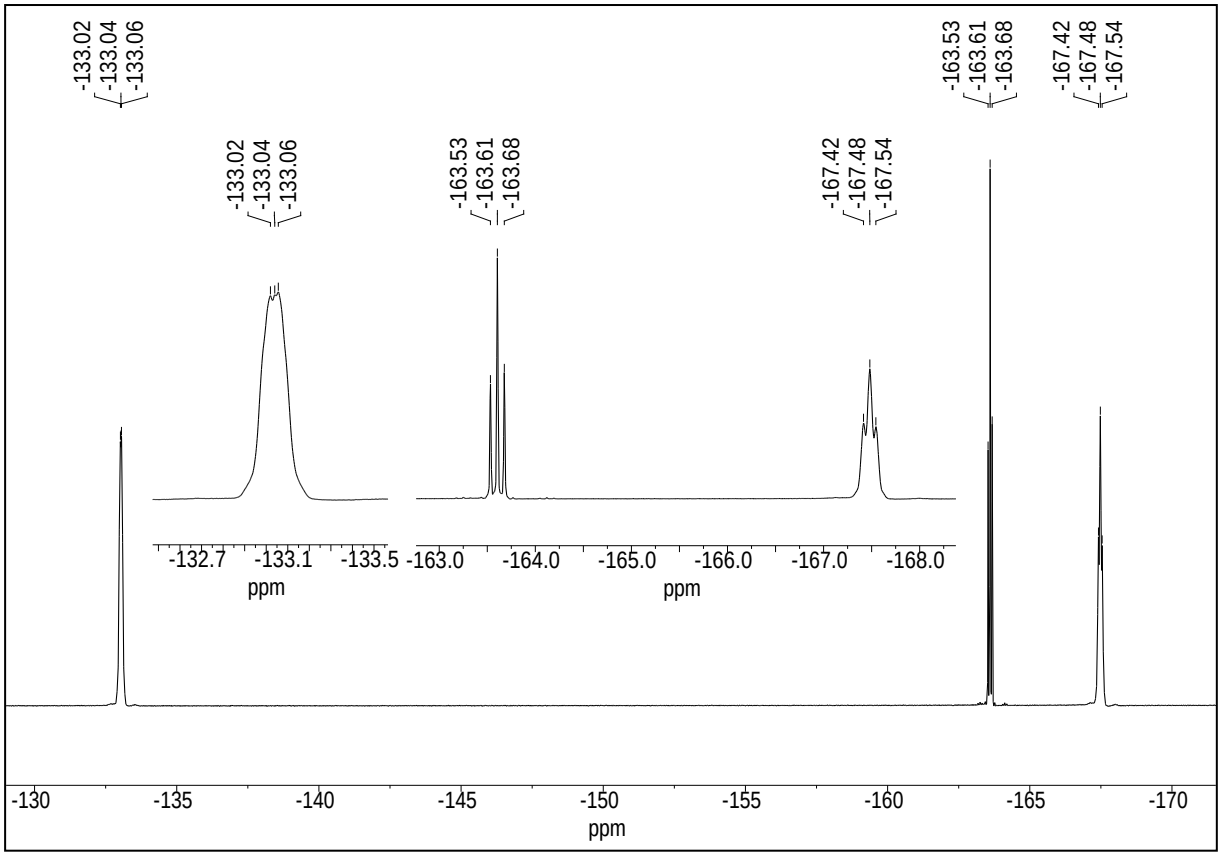

Figure S7. $^{19}F\{^{1}H\}$ NMR (282.37 MHz) spectrum of **2** in dichloromethane-d_2 at 298 K.

2.3 Synthesis of [Tp^{Me}(CO)$_2$MoSi(η^3-Cp*)] (3)

A colourless solution of **2** (270 mg, 0.32 mmol, 1.08 equiv.) in 10 mL of THF was added dropwise via a syringe to a yellow solution of Na[Tp^{Me}Mo(CO)$_2$(PMe$_3$)] (163 mg, 0.30 mmol) in 15 mL of THF at ambient temperature. Upon addition, the colour of the solution immediately changed from yellow to orange. After 20 minutes of stirring, an FT-IR spectrum of the reaction solution was recorded, which revealed the complete consumption of the metalate salt and the formation of **3** (ν_{CO} = 1849 (s) and 1772 (vs) cm^{-1}) along with a small amount of [Tp^{Me}Mo(CO)$_2$(PMe$_3$)].[S18] All volatiles were removed under vacuum and the orange residue was extracted with toluene (3 × 15 mL) at ambient temperature. The combined orange extracts were concentrated under vacuum to *ca.* 10 mL, and 20 mL of *n*-pentane were slowly added to the solution, leading to precipitation of an orange powder. The solid was separated from the yellow supernatant by filtration at ambient temperature. Recrystallization of the solid from diethyl ether (*ca.* 5 mL) at −30 °C afforded compound **3** as an analytically pure orange solid. Yield: 90 mg (0.15 mmol, 49 % from Na[Tp^{Me}Mo(CO)$_2$(PMe$_3$)]). The orange solid decomposes upon melting to a black liquid at 319 – 322 °C. Elemental analysis calcd. (%) for $C_{27}H_{37}BMoN_6O_2Si$ (612.46 g mol^{-1}): C 52.95, H 6.09, N 13.72; found: C 52.70, H 6.08, N 13.20%.

IR (*Figure S8*, THF, 298 K, cm^{-1}): ν = 1849 (s) and 1772 (vs) [ν(CO)], 1544 (w) [ν(C-C-N)$_{pz}$].

IR (fluorobenzene, 298 K, cm^{-1}): ν = 1847 (s) and 1767 (vs) [ν(CO)], 1544 (w) [ν(C-C-N)$_{pz}$].

ATR-IR (*Figures S9 and S10,* solid, ambient temperature, cm^{-1}): ν = 2981 (vw), 2918 (vw), 2862 (vw), 2525 (vw) [ν(BH)], 1846 (s) [ν(CO)], 1761 (vs) [ν(CO)], 1544 (w) [ν(C-C-N)$_{pz}$], 1479 (vw), 1447 (w), 1415 (m), 1383 (m), 1367 (w, sh), 1204 (m), 1189 (w), 1145 (vw), 1120 (vw), 1066 (w), 1045 (w), 982 (vw), 931 (vw), 872 (vw), 854 (vw), 812 (w), 795 (w), 776 (m), 696 (w), 665 (vw), 650 (w), 609 (w), 591 (m), 583 (m), 559 (m), 546 (m), 522 (w), 494 (w), 462 (w), 433 (vw).

^{1}H NMR (*Figure S11*, 300.1 MHz, benzene-d_6, 298 K, ppm): δ = 1.90 (s, 15H, C$_5$*Me*$_5$), 2.17, 2.89 (s, 3H each, C^3-*Me* and C^5-*Me*, pz$_B$), 2.21, 2.45 (s, 6H each, 2 × C^3-*Me* and 2 × C^5-*Me*, pz$_A$), ca. 4.80 (br, 1H, B*H*; this signal appears as a very broad hump over the base line in a strongly enlarged version of the spectrum), 5.47 (s, 1H, C^4-*H*, pz$_B$), 5.66 (s, 2H, 2 × C^4-*H*, pz$_A$).

[S18] The 17VE (VE = valence electrons) complex [Tp^{Me}Mo(CO)$_2$(PMe$_3$)] was synthesized independently upon one-electron reduction of [Tp^{Me}Mo(CO)$_2$(PMe$_3$)Cl] with one equivalent of sodium sand in THF at ambient temperature and isolated as a highly air-sensitive, yellow solid in 56 % yield, which was characterized by elemental analysis, IR spectroscopy and single-crystal X-ray diffraction; IR (THF, 298 K, cm^{-1}): ν = 1893 (vs) and 1756 (s) [ν(CO)], 1544 (w) [ν(C-C-N)$_{pz}$].

^{1}H NMR (*Figure S12*, 300.1 MHz, THF-d_8, 298 K, ppm) δ = 2.30 (s, 3H, 1 × C^{5}-*Me*, pz$_B$), 2.31 (s, 6H, 2 × C^{5}-*Me*, pz$_A$), 2.32 (s, 21H (15H + 6H), C$_5$*Me*$_5$ + (2 × C^{3}-*Me*), pz$_A$), 2.47 (s, 3H, 1 × C^{3}-*Me*, pz$_B$), 4.63 (br, 1H, B*H*; this signal appears as a very broad hump over the base line in a strongly enlarged version of the spectrum), 5.66 (s, 3H, C^{4}-*H*, pz$_A$ and pz$_B$).

^{13}C{^{1}H} NMR (*Figure S13*, 75.47 MHz, THF-d_8, 298 K, ppm): δ = 10.0 (s, 5C, C$_5$*Me*$_5$), 12.6 (s, 2C, 2 × C^{5}-*Me*, pz$_A$), 12.8 (s, 1C, 1 × C^{5}-*Me*, pz$_B$), 15.5 (s, 1C, 1 × C^{3}-*Me*, pz$_B$), 17.5 (s, 2C, 2 × C^{3}-*Me*, pz$_A$), 105.7 (s, 2C, 2 × *C*^{4}-H, pz$_A$), 106.2 (s, 1C, 1 × *C*^{4}-H, pz$_B$), 122.5 (s, ^{1}J(Si,C) = 13.4 Hz, 5C, *C*$_5$Me$_5$), 143.0 (s, 1C, 1 × *C*^{5}-Me, pz$_B$), 143.5 (s, 2C, 2 × *C*^{5}-Me, pz$_A$), 149.6 (s, 2C, 2 × *C*^{3}-Me, pz$_A$), 153.0 (s, 1C, 1 × *C*^{3}-Me, pz$_B$), 227.3 (s, 2C, 2 × *C*O).

^{29}Si{^{1}H} NMR: (*Figure S14*, 99.34 MHz, THF-d_8, 298K, ppm): δ = −272.4 (s).

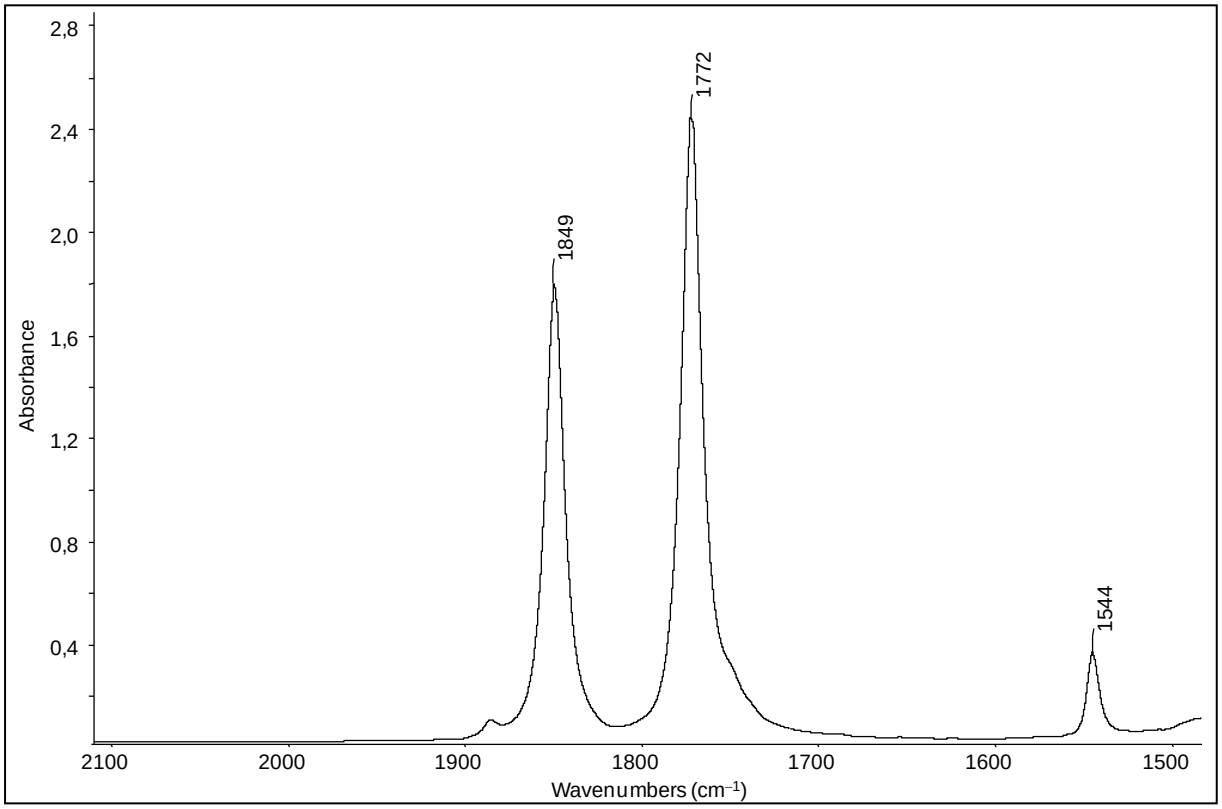

Figure S8. FT-IR spectrum (2100 – 1500 cm^{-1}) of **3** in THF at 298 K showing the characteristic ν(CO) and ν(C-C-N)$_{pz}$ absorption bands.

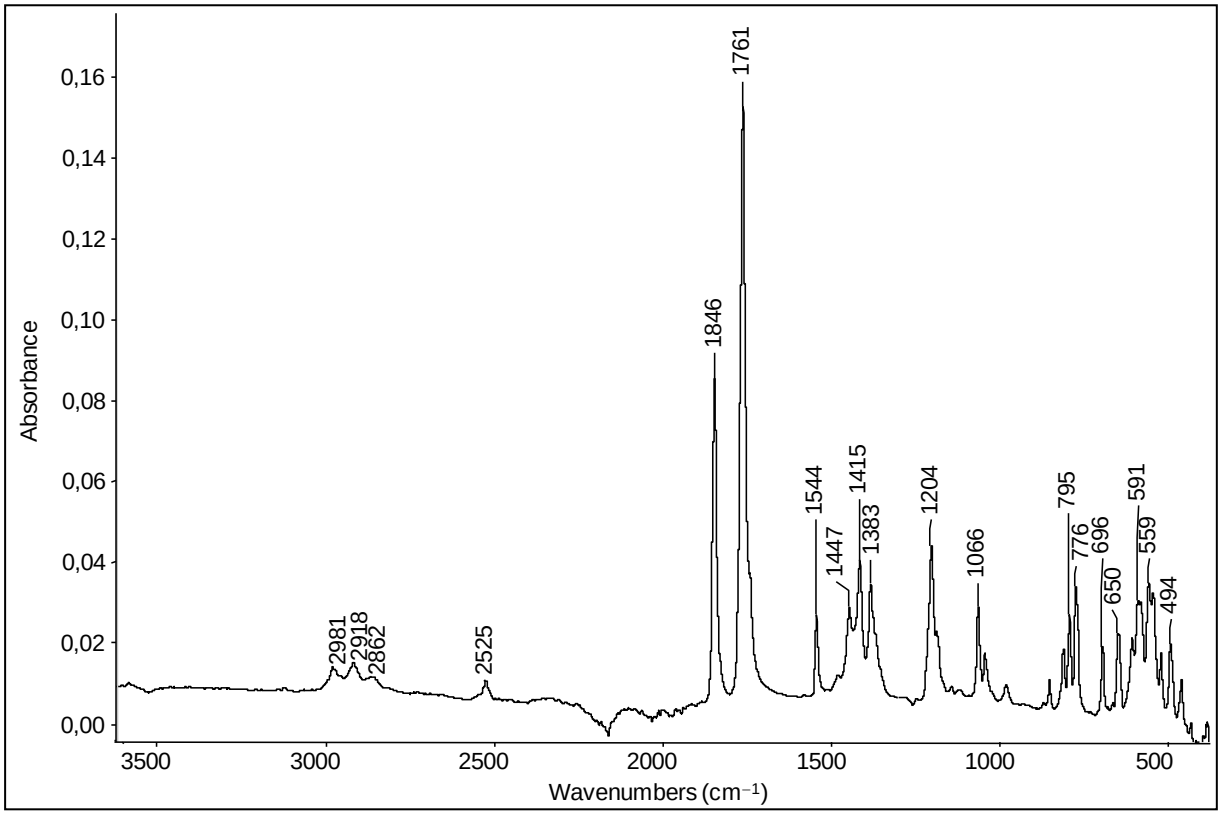

Figure S9. ATR-IR spectrum of solid **3** at ambient temperature in the range of 3600 – 400 cm^{-1}.

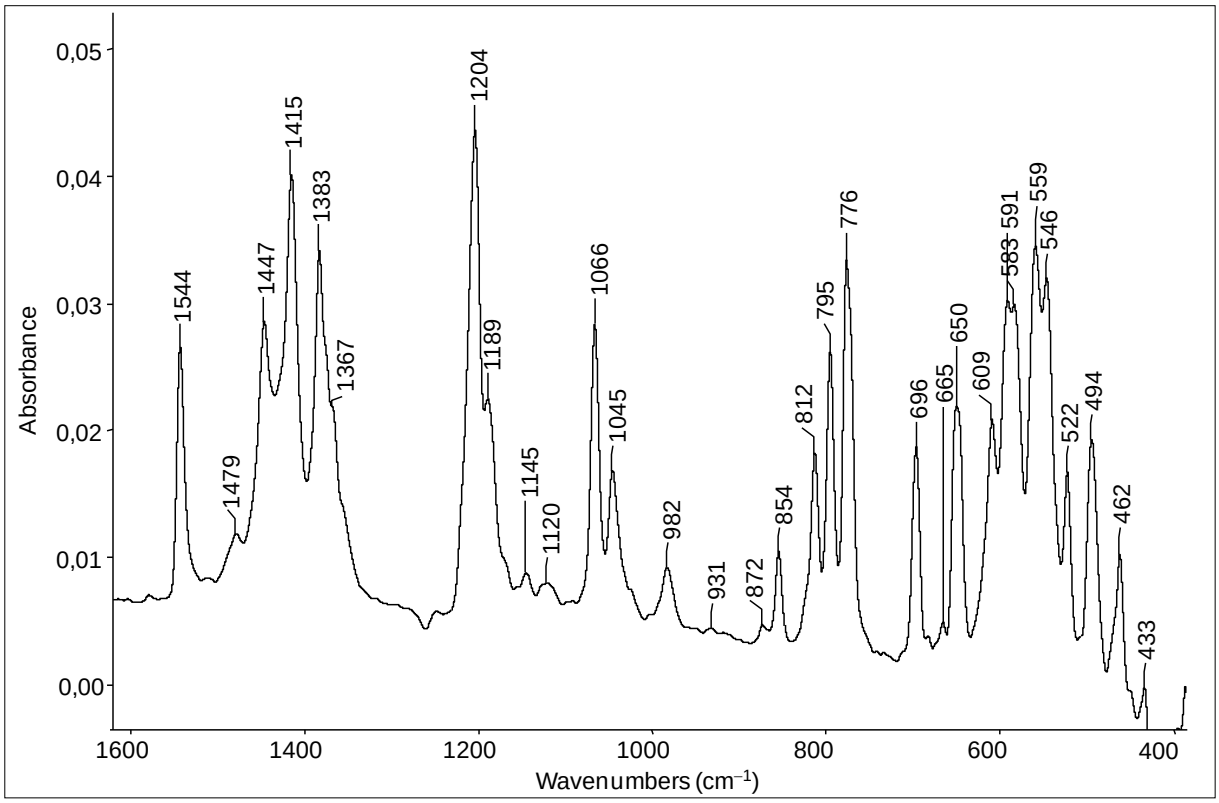

Figure S10. Excerpt (1600 – 400 cm^{-1}) of the ATR-IR spectrum of solid **3** at ambient temperature depicted in Figure S9.

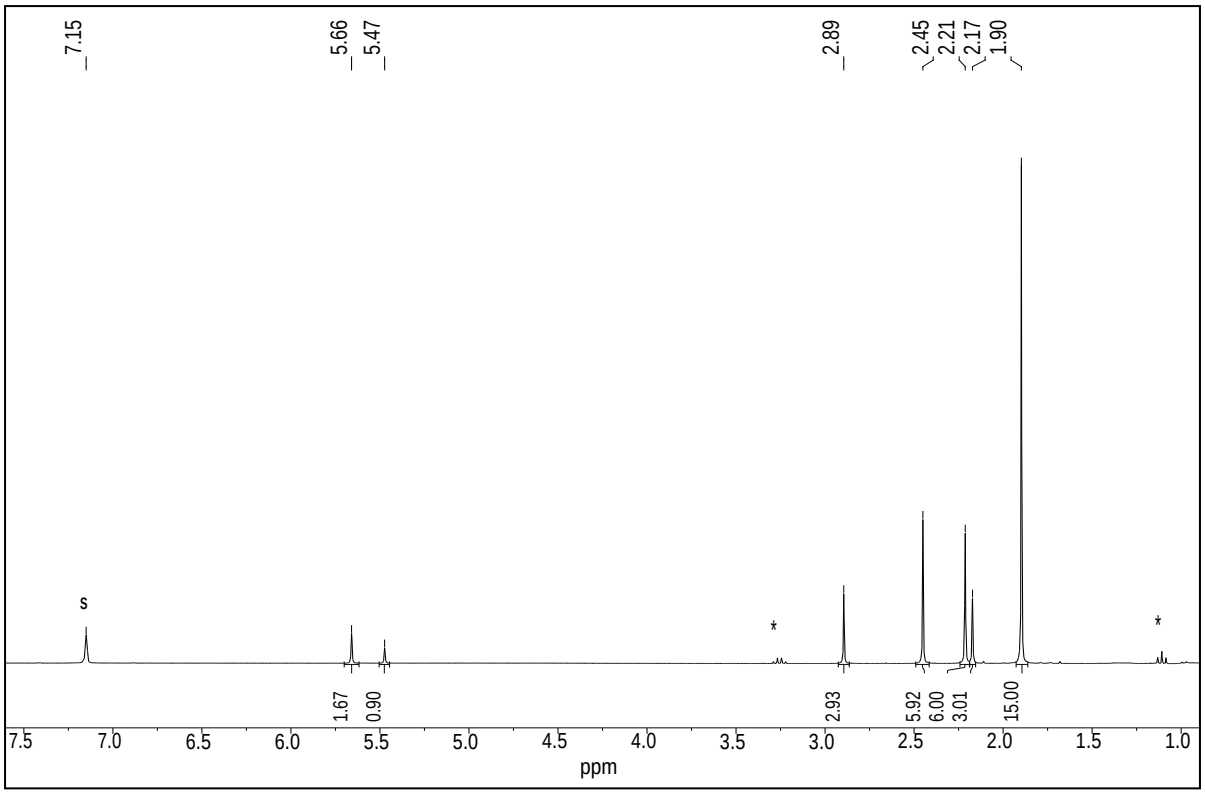

Figure S11. ^{1}H NMR spectrum (300.1 MHz) of **3** in benzene-d_6 at 298 K; the character S denotes the residual proton signal of the deuterated solvent; the signals marked with an asterisk (*) correspond to a tiny amount of diethyl ether present in the sample.

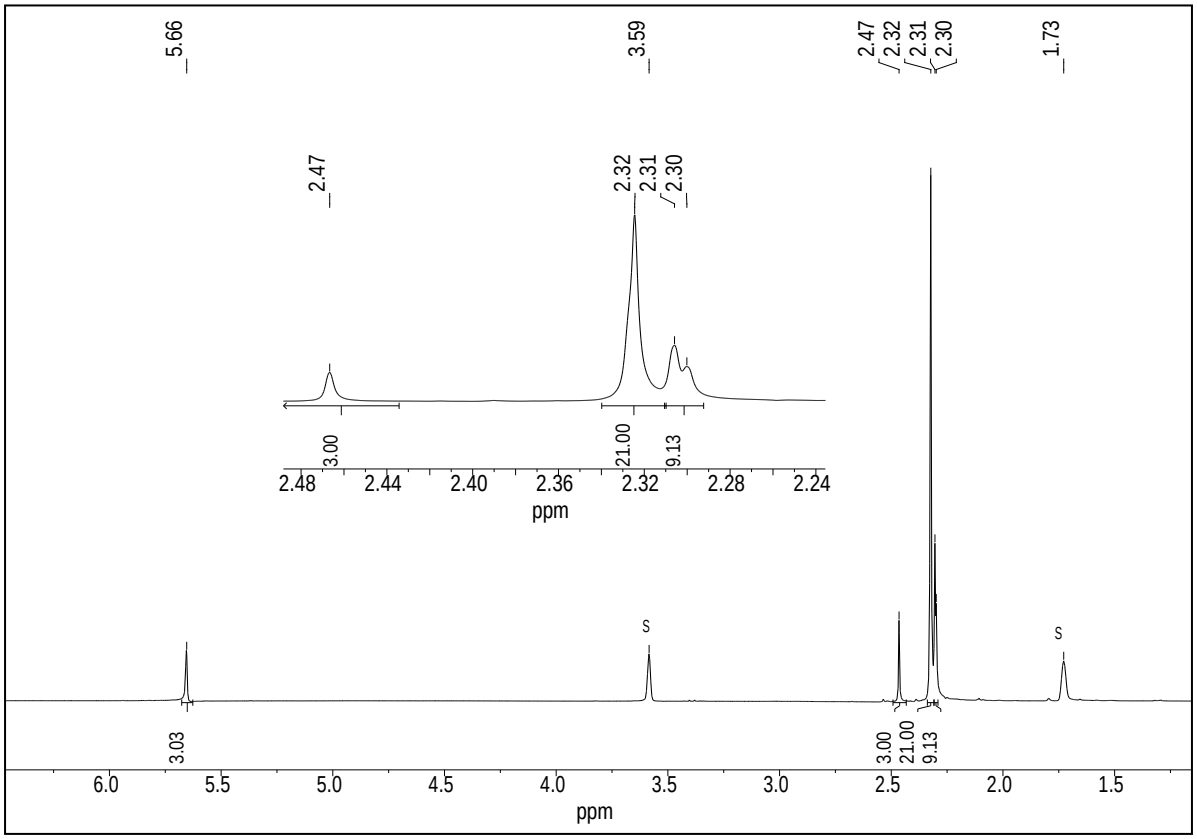

Figure S12. ^{1}H NMR spectrum (300.1 MHz) of **3** in THF-d_8 at 298 K; the character S denotes the residual proton signal of the deuterated solvent.

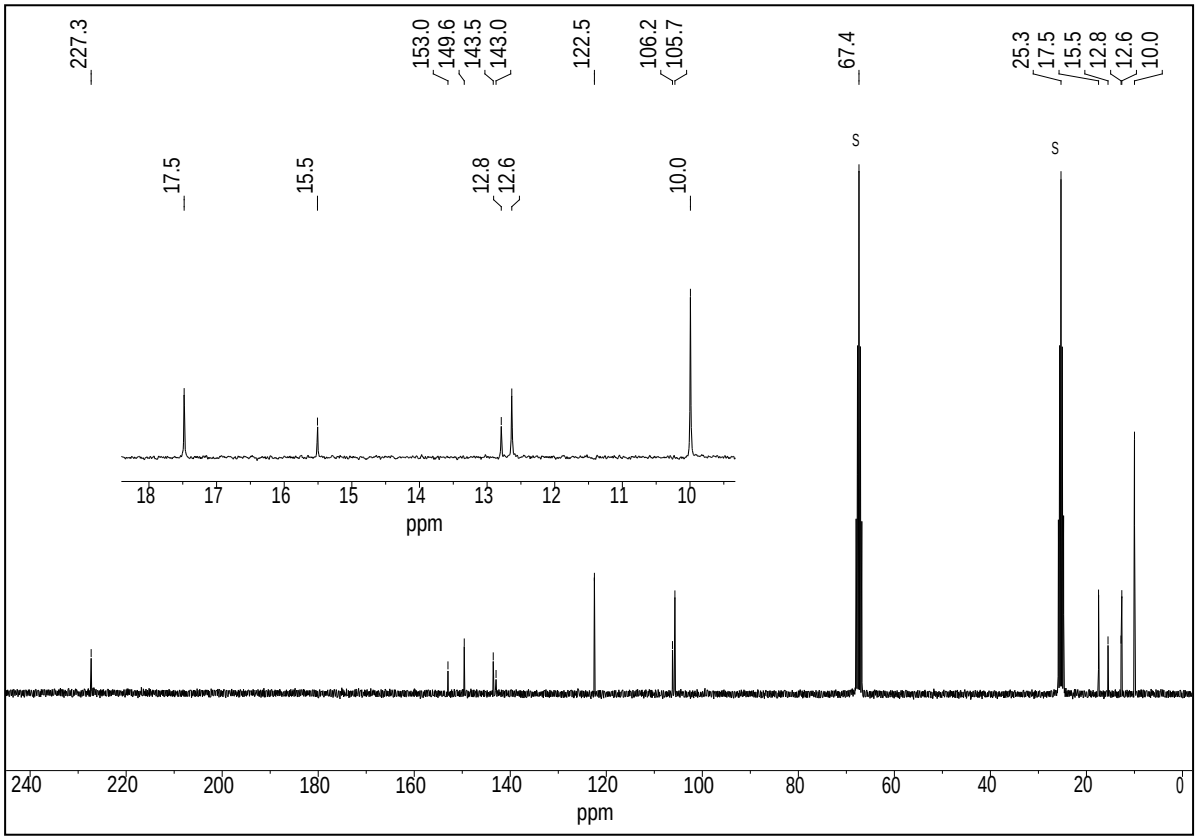

Figure S13. $^{13}C\{^1H\}$ NMR spectrum (75.47 MHz) of **3** in THF-d_8 at 298 K; the character S denotes the ^{13}C NMR signals of the deuterated solvent; an expanded section of the aliphatic region of the $^{13}C\{^1H\}$ NMR spectrum is shown in the inset.

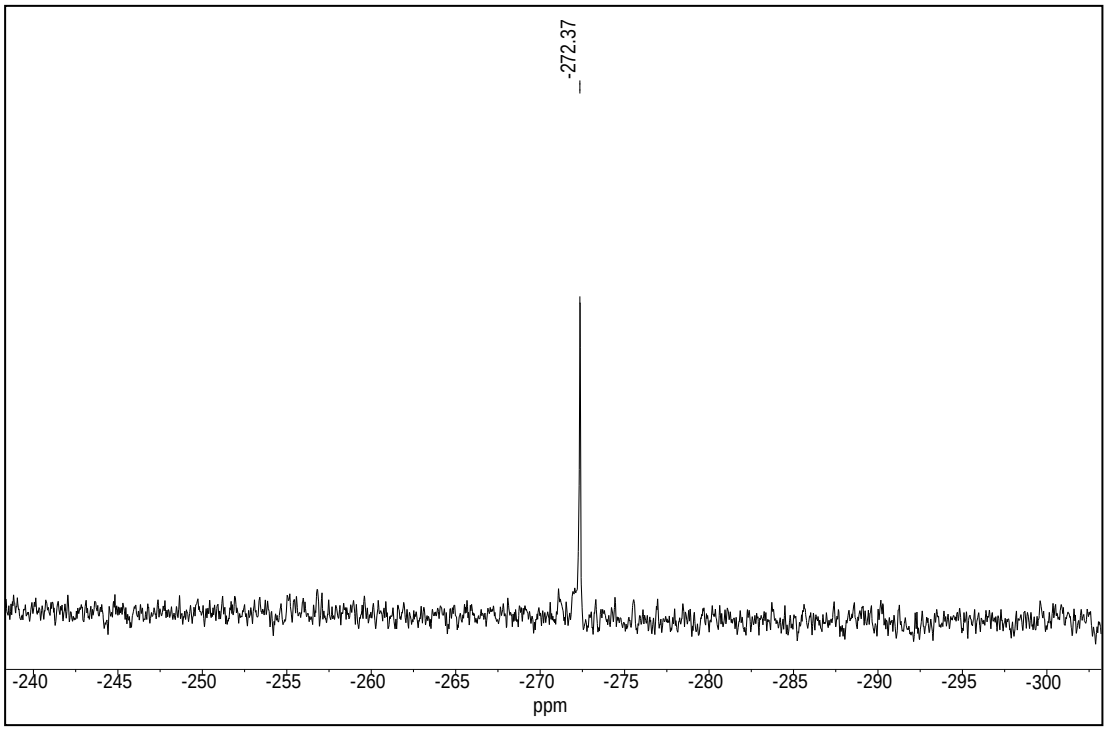

Figure S14. $^{29}Si\{^1H\}$ NMR spectrum (99.34 MHz) of **3** in THF-d_8 at 298 K.

3. Crystal structure determination

Clear orange blocks of **3** for single-crystal X-ray diffraction were obtained by slow evaporation of a concentrated benzene solution of **3** at ambient temperature.

The data collection for **3** was performed on a STOE IPDS-2T diffractometer (area detector) using graphite monochromated Mo-K_α irradiation (λ = 0.71073 Å). The diffractometer was equipped with a low-temperature device (Oxford Cryostream 700er series, Oxford Cryosystems, 123(2) K). Intensities were measured by fine-slicing ω and φ-scans and corrected for background, polarization and Lorentz effects. The absorption correction for **3** was performed by integration. The structures were solved by direct methods and refined anisotropically by the least-square procedure implemented in the SHELX program system.[S19] Hydrogen atoms were included isotropically using the riding model on the bound carbon atoms and the boron atom.

CCDC number 1563754 contains the supplementary crystallographic data for this paper, which can be obtained free of charge from the Cambridge Crystallographic Data Centre via www.ccdc.cam.ac.uk/data_request/cif.

Table S1: Crystal data and refinement for **3**.

Empirical formula	$C_{27}H_{37}BMoN_6O_2Si$
Moiety formula	$C_{27}H_{37}BMoN_6O_2Si$
Formula weight	612.46 g mol^{-1}
Temperature	123(2) K
Wavelength	0.71073 Å
Crystal system, space group	monoclinic, $P2_1/n$
Unit cell dimensions	a = 12.0512(2) Å, α = 90°
	b = 18.3946(5) Å, β = 90.0420(10)°
	c = 13.0909(2) Å, γ = 90°
Volume	2901.95(10) Å^3
Z, Calculated density	4, 1.402 mg m^{-3}
Absorption coefficient	0.528 mm^{-1}
F(000)	1272
Crystal size	0.18 × 0.12 × 0.09 mm
θ-range for data collection	2.707 – 26.997
Limiting indices	$-13 \le h \le 15$, $-23 \le k \le 23$, $-16 \le l \le 16$
Reflections collected / unique	38375 / 6333 [R_{int} = 0.0285]
Completeness to θ = 25.25°	99.9 %
Absorption correction	Integration
Max. and min. transmission	0.9786 and 0.8564
Refinement method	Full-matrix least squares on F^2
Data / restraints / parameters	6333 / 0 / 355
Goodness-of-fit on F^2	0.939
Final R indices [$I > \sigma(I)$]	R_1 = 0.0168, wR_2 = 0.0388
R indices (all data)	R_1 = 0.0200, wR_2 = 0.0391
Largest diff. peak / hole	0.23 / −0.24 e Å^{-3}

[S19] Sheldrick, G. M. *SHELXS97* and *SHELXL97*, University of Göttingen, Germany, **1997**.

4. Electronic structure calculations

The structure optimization of $\mathbf{3_{calc}}$ was performed with the TURBOMOLE 7.0 program[S20] using the TPSSh-D3 functional,[S21] including the RI approximation,[S22] in combination with the def2-TZVP basis set for all atoms.[S23] The cartesian coordinates of the solid state structure of **3** were used as a starting point for the structure optimization. The optimized geometry of $\mathbf{3_{calc}}$ was verified as minimum on the potential energy surface by two-sided numerical differentiation of the analytical gradients to obtain the harmonic frequencies, which were also used to calculate the zero point vibrational energy (ZPVE). The natural bond orbital (NBO) and natural resonance theory (NRT) analyses of $\mathbf{3_{calc}}$ were performed using the NBO 6.0 program.[S24]

The NRT bond orders of the C-C bonds of the Cp* ring of $\mathbf{3_{calc}}$ (Fig. S18) have been obtained via a separate local multi-reference NRT analysis including the atoms Si, C1, C2, C3, C4, and C5 due to limitations of the allowed number of reference structures during the full NRT analysis of $\mathbf{3_{calc}}$.

[S20] (a) Ahlrichs, R.; Bär, M.; Häser, M.; Horn, H.; Kölmel, C. *Chem. Phys. Lett.* **1989**, *162*, 165. (b) TURBOMOLE Version 7.0, a development of University of Karlsruhe and Forschungszentrum GmbH Karlsruhe, **1989** – **2007**; TURBOMOLE GmbH, since **2007**. (c) Furche, F.; Ahlrichs, R.; Hättig, C.; Klopper, W.; Sierka, M.; Weigend, F. *WIREs Comput. Mol. Sci*. **2014**, *4*, 91.

[S21] (a) Tao, J.; Perdew, J. P.; Staroverov, V. N.; Scuseria, G. E. *Phys. Rev. Lett.* **2003**, *91*, 146401. (b) Grimme, S., *J. Comp. Chem*. **2006**, *27*, 1787. (c) Grimme, S.; Antony, J.; Ehrlich, S.; Krieg, H. *J. Chem. Phys*. **2010**, *132*, 154104. (d) Grimme, S.; Ehrlich, S.; Goerigk, L. *J. Comp. Chem*. ***2011***, *32*, 1456.

[S22] (a) Neese, F. *J. Comput. Chem.* **2003**, *24*, 1740. (b) Neese, F.; Wennmohs, F.; Hansen, A.; Becker, U. *Chem. Phys.* **2009**, *356*, 98.

[S23] (a) Schäfer, A.; Horn, H.; Ahlrichs, R. *J. Chem. Phys*. **1992**, *97*, 2571. (b) Weigend, F.; Ahlrichs, R. *Phys. Chem. Chem. Phys.* **2005**, *7*, 3297.

[S24] NBO 6.0 Program. Glendening, E. D.; Badenhoop, J. K.; Reed, A. E.; Carpenter, J. E.; Bohmann, J. A.; Morales, C. M.; Landis, C. R.; Weinhold, F. Theoretical Chemistry Institute, University of Wisconsin, Madison, WI, **2013**.

4.1 Comparison of selected bonding parameters of 3 and 3_{calc}

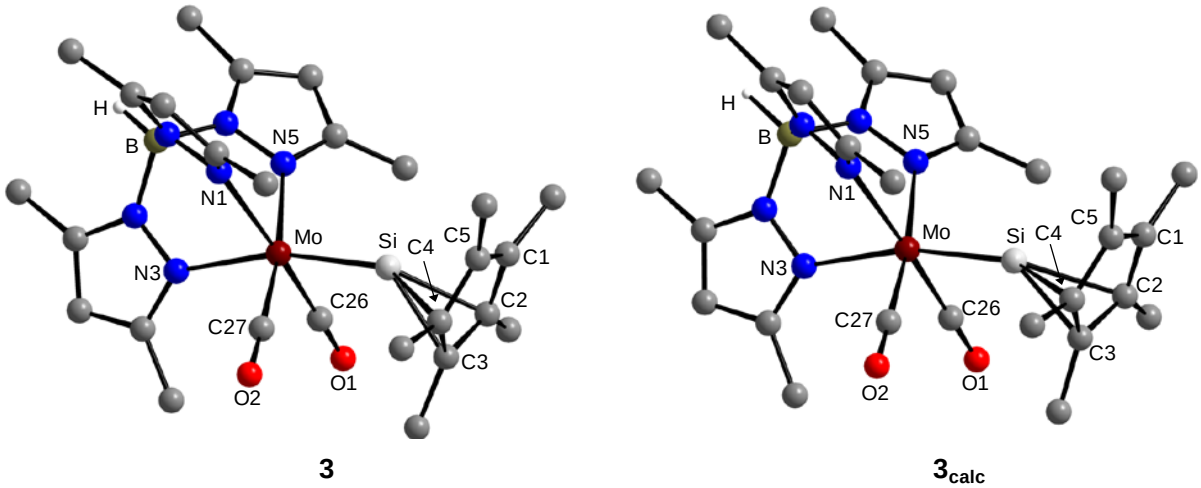

Figure S15. Experimental (left) and calculated (right) structures of **3**; the H atoms except the B-bonded H atom are omitted for clarity; atom numbering of the experimental structure was taken over in the calculated structure.

Table S2: Comparison of selected experimental bond lengths [Å] and angles [°] of **3** with the calculated bond lengths and angles of $\mathbf{3}_{calc}$; atom numbering of the experimental structure was taken over in the calculated structure.

	Mo–Si	Mo–N1	Mo–N3	Mo–N5	Mo–C26	Mo–C27	C26–O1
3	2.3092(4)	2.281(2)	2.217(1)	2.252(2)	1.929(2)	1.938(2)	1.172(2)
$\mathbf{3}_{calc}$	2.286	2.275	2.231	2.275	1.956	1.956	1.174
	C27–O2	Si–C1	Si–C2	Si–C3	Si–C4	Si–C5	C1–C2
3	1.176(2)	2.318(2)	2.171(2)	2.078(2)	2.158(2)	2.302(2)	1.421(3)
$\mathbf{3}_{calc}$	1.174	2.303	2.177	2.092	2.177	2.303	1.426
	C1–C5	C2–C3	C3–C4	C4–C5	Si–C_f[a]	Si–C_g[b]	N1-Mo-Si
3	1.413(2)	1.428(3)	1.443(3)	1.422(3)	1.8283(9)	1.844(1)	109.46(4)
$\mathbf{3}_{calc}$	1.423	1.439	1.439	1.426	1.834	1.847	106.18
	N3-Mo-Si	N5-Mo-Si	C26-Mo-Si	C27-Mo-Si	Mo-Si-C1	Mo-Si-C2	Mo-Si-C3
3	164.30(3)	107.90(4)	78.55(6)	79.12(6)	157.85(7)	138.94(6)	130.61(5)
$\mathbf{3}_{calc}$	169.01	106.18	79.64	79.64	156.57	141.28	133.36
	Mo-Si-C4	Mo-Si-C5	Mo-Si-C_f[a]	Mo-Si-C_g[b]			
3	140.34(6)	159.18(6)	158.5(1)	166.0(1)			
$\mathbf{3}_{calc}$	141.28	156.57	162.1	168.8			

[a]: Si–C_f is the distance between the silicon atom and the foot C_f of the silicon-to ring-normal on the Cp* ring plane; it is the shortest distance between Si and the Cp* ring plane. [b]: Si–C_g is the distance between the silicon atom and the center of gravity (C_g) of the Cp* ring.

Table S3: Comparison of the experimental and calculated angles α between the methyl groups and the C_5 ring plane of the Cp* substituents of **3** and $\mathbf{3}_{calc}$; atom numbering of the experimental structure was taken over in the calculated structure.

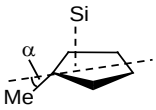	α(C1-Me)	α(C2-Me)	α(C3-Me)	α(C4-Me)	α(C5-Me)
3	1.0(2)	1.0(1)	2.8(1)	1.3(1)	−0.4(2)
$\mathbf{3}_{calc}$	−2.48	0.62	1.82	0.62	−2.48

4.2 Selected Kohn-Sham orbitals of 3_{calc}

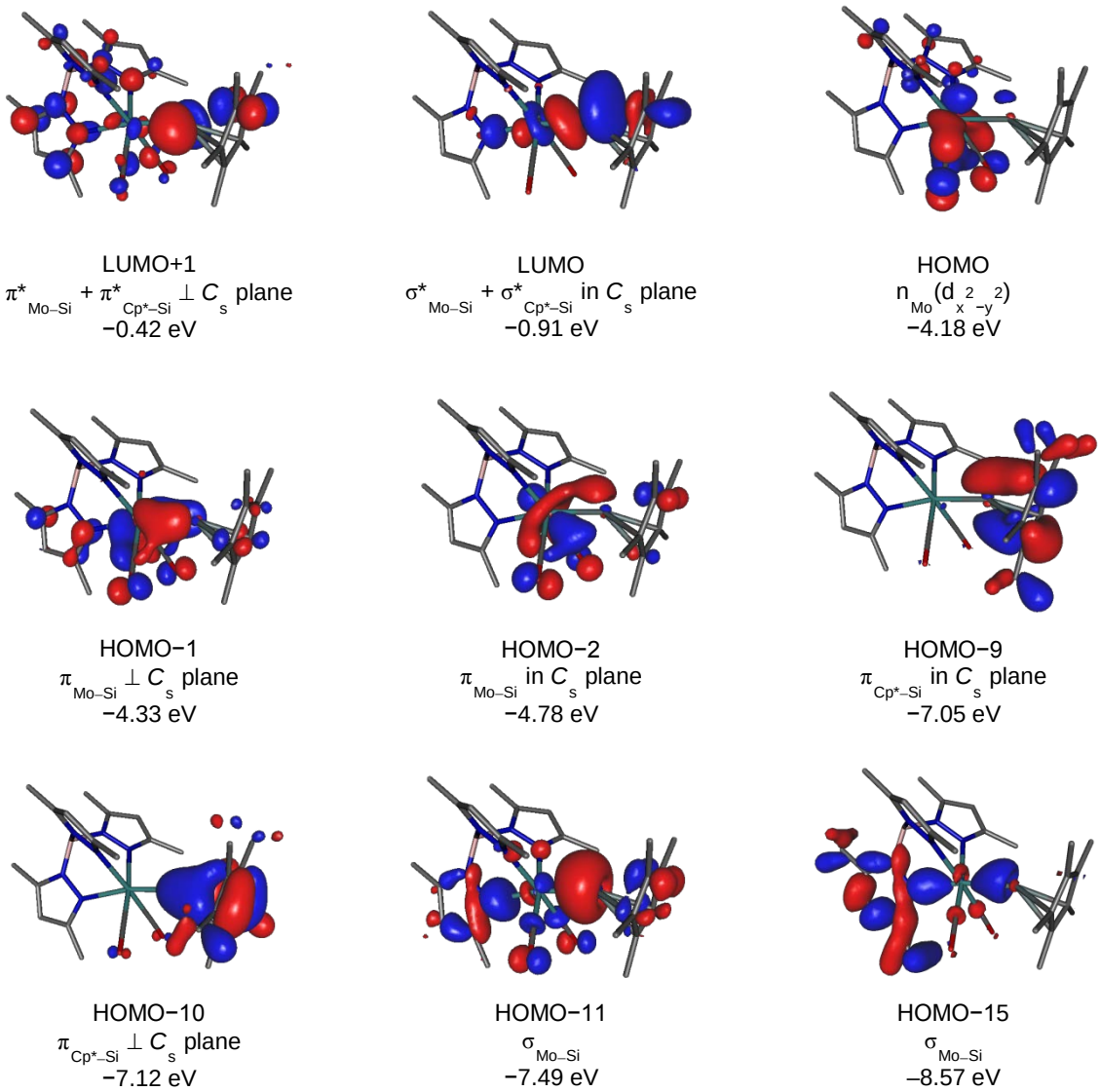

Figure S16. Selected *Kohn-Sham* orbitals of $\mathbf{3_{calc}}$ at the RI-TPSSh-D3/def2-TZVP level of theory and their corresponding energy eigenvalues; isosurface value: 0.04 e bohr^{-3}.

4.3 Selected results of the NBO and NRT analyses of 3_{calc}

Table S4: Selected results of the natural bond orbital (NBO) analysis of $\mathbf{3}_{calc}$; atom numbering of the experimental structure was taken over in the calculated structure.[a – c]

NBO analysis[a,c]					NPA partial charges[b]	
	occ.	pol. [%]	hyb.	WBI		
σ(Mo–Si)	1.94	23.4 (Mo) 76.6 (Si)	$sd^{1.55}$ (Mo) $sp^{0.11}$ (Si)	1.03	Mo	−0.57
π_1(Mo–Si)	1.65	83.5 (Mo) 16.5 (Si)	d (Mo) p (Si)		Si	1.13
π_2(Mo–Si)	1.41	98.8 (Mo) 1.2 (Si)	d (Mo) $sp^{14.92}d^{2.01}$ (Si)		Cp*	−0.33
LP(Mo)	1.46		d			
LP(C1)	1.06		p			
3c(Si-C2-C3)	1.67	3.5 (Si) 45.9 (C2) 50.6 (C3)	$sp^{14.71}d^{23.94}$ (Si) p (C2) p (C3)			
3c(Si-C4-C5)	1.71	5.7 (Si) 46.8 (C4) 47.6 (C5)	$sp^{30.77}d^{9.02}$ (Si) p (C4) p (C5)			
σ*(Mo–Si)	0.34	76.6 (Mo) 23.4 (Si)	$sd^{1.55}$ (Mo) $sp^{0.11}$ (Si)			
π^*_1(Mo–Si)	0.25	16.5 (Mo) 83.5 (Si)	d (Mo) p (Si)			
π^*_2(Mo–Si)	0.38	1.2 (Mo) 98.8 (Si)	d (Mo) $sp^{14.92}d^{2.01}$ (Si)			
3c*(Si-C2-C3)	0.59	6.0 (Si) 52.1 (C2) 47.5 (C3)	$sp^{14.71}d^{23.94}$ (Si) p (C2) p (C3)			
3c*(Si-C2-C3)	0.03	96.5 (Si) 1.6 (C2) 1.9 (C3)	$sp^{14.71}d^{23.94}$ (Si) p (C2) p (C3)			
3c*(Si-C4-C5)	0.52	2.3 (Si) 53.0 (C4) 44.8 (C5)	$sp^{30.77}d^{9.02}$ (Si) p (C4) p (C5)			
3c*(Si-C4-C5)	0.15	92.1 (Si) 0.3 (C4) 7.6 (C5)	$sp^{30.77}d^{9.02}$ (Si) p (C4) p (C5)			

[a]: occ.: occupancy, pol.: polarization, hyb.: hybridization, WBI: Wiberg bond index, LP = lone pair, 3c = three-center bond. [b]: Partial charges obtained by natural population analysis (NPA); [c] As the NBO analysis interprets the wave function in terms of one Lewis structure featuring two and three center bonds; the overall C_s symmetry of the wave function (mirror plane is build up by the atoms Mo, Si, and C3) is not reflected in the above NBO results. A second NBO structure with interchanged atoms C1 by C5, as well as C2 by C4 features the same weight.

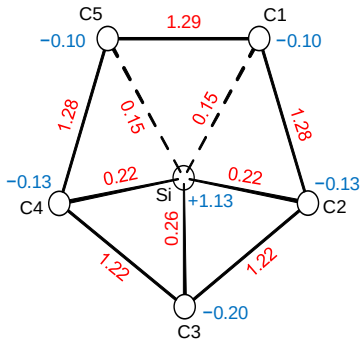

Figure S17. Wiberg bond indices (red) and partial charges (blue) of the Si–Cp* fragment.

Table S5: Selected results of the second order perturbation theory analysis of the Fock matrix in the NBO basis of **3**$_{calc}$; atom numbering of the experimental structure was taken over in the calculated structure.

Donor orbital	Acceptor orbital	Interaction energy [kcal mol^{-1}]
LP(Mo)	π^*_2(Mo–Si)	18.00
LP(C1)	3c*(Si-C2-C3)	108.75
LP(C1)	3c*(Si-C4-C5)	93.03
3c(Si-C2-C3)	σ^*(Mo–Si)	2.12
3c(Si-C2-C3)	π^*_1(Mo–Si)	8.53
3c(Si-C2-C3)	π^*_2(Mo–Si)	76.37
3c(Si-C4-C5)	σ^*(Mo–Si)	5.20
3c(Si-C4-C5)	π^*_1(Mo–Si)	20.24
LP(N3)	σ^*(Mo–Si)	64.67

The natural resonance theory (NRT) analysis of **3**$_{calc}$ revealed in total 46 resonance structures contributing with more than 0.1% to the resonance hybrid, which is in agreement with a highly delocalized structure of **3**$_{calc}$. Out of these structures, 18 structures contain a Mo–Si triple bond (63.8 % contribution), 11 structures contain a Mo–Si double bond (10.2 % contribution) and 12 structures contain a Mo–Si single bond (23.3 % contribution). Four structures contain no Mo–Si bond (2.1 % contribution). The total Mo–Si NRT bond order amounts to 2.37, comprising covalent and ionic contributions of 0.94 and 1.43, respectively. The calculated NRT bond orders of the Si–Cp* fragment (Figure S18) suggest a bonding between the Si atom and the Cp* ring which is mainly driven by electrostatic interactions. This is, for example, in full agreement to the low calculated barrier (14.8 kJ mol^{-1}) for the haptotropic shift via an η^4-coordinated transition state to the next η^3-coordinated rotamer (see Chapter 4.4).

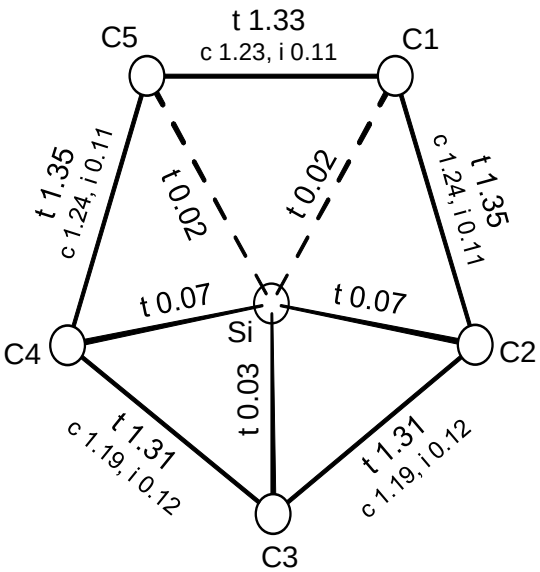

Figure S18. NRT bond orders of the Si–Cp* fragment; only the total NRT bond order is given for the Si–C bonds, which are fully ionic according to the NRT analysis; t = total, c = covalent, i = ionic.

4.4 Calculation of the PES of the haptotropic shift of 3

A scan of the potential energy surface (PES) of $\mathbf{3}_{\mathbf{calc}}$ revealed the presence of a η^4-coordinated transition state ($\mathbf{3}_{\mathbf{calc}}^{\mathbf{TS}}$), which interconnects two isoenergetic global η^3-coordinated minimum structures (Figure S19). The transition state $\mathbf{3}_{\mathbf{calc}}^{\mathbf{TS}}$ was found to be 14.8 kJ mol^{-1} higher in energy than the global minimum structure and displays one imaginary frequency with a magnitude of −27.6 cm^{-1}, which comprises a rotation of the Cp* ring about the Si–Cp* vector. This rationalizes the rapid haptotropic shift of **3** observed by variable-temperature ^{1}H and ^{13}C NMR spectroscopy even at −80 °C. A comparison of selected structural parameters of the minimum structure $\mathbf{3}_{\mathbf{calc}}$ and the transition state $\mathbf{3}_{\mathbf{calc}}^{\mathbf{TS}}$ is provided in Tables S6 and S7.

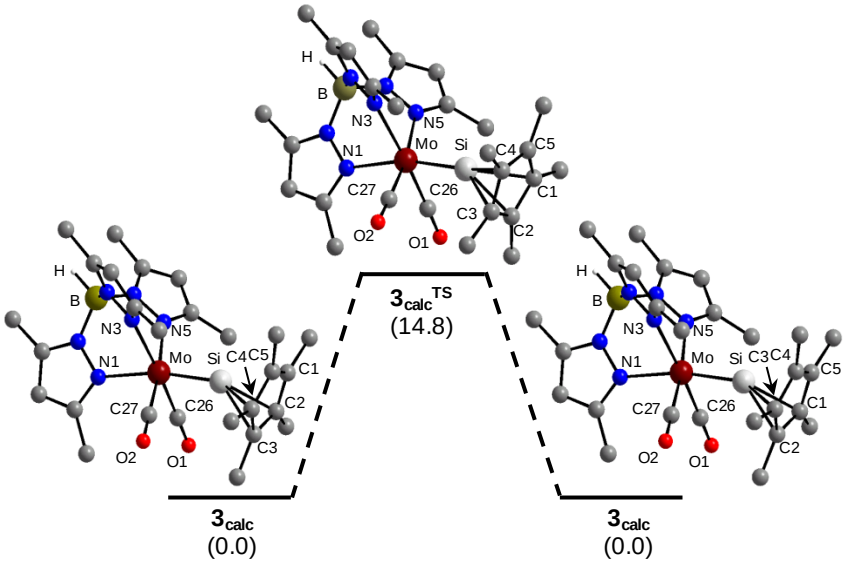

Figure S19. Calculated PES of the haptotropic shift of $\mathbf{3}_{\mathbf{calc}}$ via the transition state $\mathbf{3}_{\mathbf{calc}}^{\mathbf{TS}}$; relative energies are given in brackets in kJ mol^{-1}; the H atoms except the B-bonded H atom are omitted for clarity; atom numbering of the experimental structure was taken over in the calculated structures.

Table S6: Comparison of selected bond lengths [Å] and angles [°] of $\mathbf{3}_{\mathbf{calc}}$ and $\mathbf{3}_{\mathbf{calc}}^{\mathbf{TS}}$; atom numbering of the experimental structure was taken over in the calculated structures.

	Mo–Si	Mo–N1	Mo–N3	Mo–N5	Mo–C26	Mo–C27	C26–O1
$\mathbf{3}_{\mathbf{calc}}$	2.286	2.275	2.231	2.275	1.956	1.956	1.174
$\mathbf{3}_{\mathbf{calc}}^{\mathbf{TS}}$	2.297	2.280	2.235	2.280	1.959	1.959	1.172
	C27–O2	Si–C1	Si–C2	Si–C3	Si–C4	Si–C5	C1–C2
$\mathbf{3}_{\mathbf{calc}}$	1.174	2.303	2.177	2.092	2.177	2.303	1.426
$\mathbf{3}_{\mathbf{calc}}^{\mathbf{TS}}$	1.172	2.286	2.129	2.129	2.286	2.377	1.432
	C1–C5	C2–C3	C3–C4	C4–C5	Si–C_f[a]	Si–C_g[b]	N1-Mo-Si
$\mathbf{3}_{\mathbf{calc}}$	1.423	1.439	1.439	1.426	1.834	1.847	106.18
$\mathbf{3}_{\mathbf{calc}}^{\mathbf{TS}}$	1.422	1.439	1.426	1.432	1.867	1.885	107.61
	N3-Mo-Si	N5-Mo-Si	C26-Mo-Si	C27-Mo-Si	Mo-Si-C1	Mo-Si-C2	Mo-Si-C3
$\mathbf{3}_{\mathbf{calc}}$	169.01	106.18	79.64	79.64	156.57	141.28	133.36
$\mathbf{3}_{\mathbf{calc}}^{\mathbf{TS}}$	166.91	107.61	80.26	80.26	149.67	137.79	137.79
	Mo-Si-C4	Mo-Si-C5	Mo-Si-C_f[a]	Mo-Si-C_g[b]			
$\mathbf{3}_{\mathbf{calc}}$	141.28	156.57	162.1	168.8			
$\mathbf{3}_{\mathbf{calc}}^{\mathbf{TS}}$	149.67	158.56	163.2	171.1			

[a]: Si–C_f is the distance between the silicon atom and the foot C_f of the silicon-to ring-normal on the Cp* ring plane; it is the shortest distance between Si and the Cp* ring plane. [b]: Si–C_g is the distance between the silicon atom and the center of gravity (C_g) of the Cp* ring.

Table S7: Comparison of the calculated angles α between the methyl groups and the Cp* ring plane in $\mathbf{3}_{\mathbf{calc}}$ and $\mathbf{3}_{\mathbf{calc}}^{\mathbf{TS}}$; atom numbering of the experimental structure was taken over in the calculated structure.

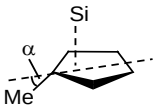	α(C1-Me)	α(C2-Me)	α(C3-Me)	α(C4-Me)	α(C5-Me)
$\mathbf{3}_{\mathbf{calc}}$	−2.48	0.62	1.82	0.62	−2.48
$\mathbf{3}_{\mathbf{calc}}^{\mathbf{TS}}$	1.15	3.98	3.98	1.15	−3.28

4.5 Calculated structure and NBO and NRT analyses of $[Si(\eta^5\text{-}Cp^*)]^+$

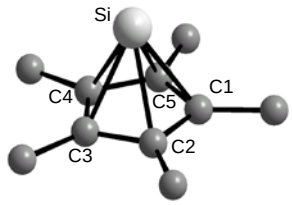

Figure S20. Calculated minimum structure (RI-TPSSh-D3/def2-TZVP) of $[Si(\eta^5\text{-}Cp^*)]^+$.

Table S8: Comparison of experimental and calculated bond lengths [Å] of $[Si(\eta^5\text{-}Cp^*)]^+$.

	exp.[b]	calc.
Si–C1	2.160(2)	2.141
Si–C2	2.148(2)	2.141
Si–C3	2.139(2)	2.141
Si–C4	2.142(2)	2.141
Si–C5	2.147(2)	2.141
C1–C2	1.442(3)	1.437
C2–C3	1.436(3)	1.437
C3–C4	1.439(3)	1.437
C4–C5	1.443(3)	1.437
C1–C5	1.430(3)	1.437
Si–C_g[a]	1.765(1)	1.758

[a]: C_g = center of gravity of the Cp* ring. [b]: Data taken from: Jutzi, P.; Mix, A.; Rummel, B.; Schoeller, W. W.; Neumann, B.; Stammler, H.-G. *Science* **2004**, *305*, 849.

Table S9: Selected results of the NBO and NRT analyses of $[Si(\eta^5\text{-}Cp^*)]^+$.

NBO analysis[a]				NPA partial charges[b]		NRT analysis[c]	
	occ.	hyb.	WBI				tot / cov / ionic
LP(Si)	2.00	$sp^{0.13}$		Si	0.89	Si–C_{ring}	0.39 / 0.13 / 0.25
Si–C_{ring}			0.34	C_{ring}	−0.10	C_{ring}–C_{ring}	1.12 / 1.09 / 0.03
C_{ring}–C_{ring}			1.22	Cp*	0.11		

[a]: occ.: occupancy, hyb.: hybridization, WBI: Wiberg bond index. [b]: Partial charges obtained by natural population analysis (NPA). [c]: tot.: total, cov.: covalent.

4.6 Calculated structure and NBO and NRT analyses of $[Cp^*(CO)_2FeSi(\eta^3\text{-}Cp^*)]$

For comparison the geometry of the ferriosilylene $[Cp^*(CO)_2FeSi(\eta^3\text{-}Cp^*)]$ was calculated at the same level of theory as that used for $\mathbf{3_{calc}}$ and the $[Si(\eta^5\text{-}Cp^*)]^+$ ion and its electronic structure studied by NBO and NRT analysis. The results are listed in Tables S10 – S12.

Table S10: Comparison of selected experimental and calculated bond lengths [Å] of [Cp*(CO)$_2$FeSi(η^3-Cp*)]; the same atom numbering scheme was used for the ring carbon atoms as for **3**.

	Fe–Si	Si–C1	Si–C2	Si–C3	Si–C4	Si–C5
[Cp*(CO)$_2$FeSiCp*]$_{exp}$[a]	2.3677(6)	2.732(2)	2.435(2)	2.136(2)	2.210(2)	2.583(2)
[Cp*(CO)$_2$FeSiCp*]$_{calc}$	2.343	2.787	2.436	2.161	2.336	2.733
	C1–C2	C2–C3	C3–C4	C4–C5	C5–C1	
[Cp*(CO)$_2$FeSiCp*]$_{exp}$[a]	1.409(3)	1.436(3)	1.434(3)	1.424(3)	1.396(3)	
[Cp*(CO)$_2$FeSiCp*]$_{calc}$	1.419	1.443	1.446	1.423	1.402	

[a]: Data taken from: Jutzi, P.; Leszczyńska, K.; Mix, A.; Neumann, B.; Rummel, B.; Schoeller, W.; Stammler, H.-G. *Organometallics* **2010**, *29*, 4759.

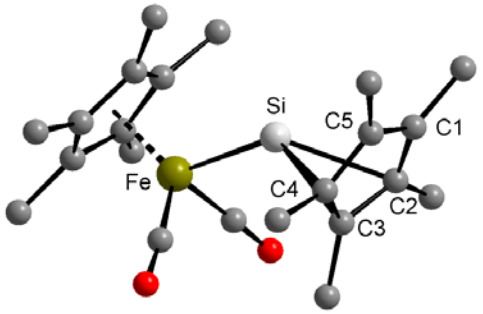

Figure S21. Experimental structure and numbering scheme used for [Cp*(CO)$_2$FeSi(η^3-Cp*)].

Table S11: Selected results of the NBO and NRT analyses of [Cp*(CO)$_2$FeSi(η^3-Cp*)]$_{calc}$.

NBO analysis[a]					NPA partial charges[b]		NRT analysis[c]
	occ.	pol. [%]	hyb.	WBI			tot / cov / ionic
σ(Fe–Si)	1.60	76.6 (Fe) 23.4 (Si)	sd$^{3.44}$ (Fe) sp$^{13.28}$ (Si)	0.45	Fe	−0.47	0.87/0.41/0.46
Si-C1				0.06	Si	0.70	0.00/0.00/0.00
Si-C2				0.23	Cp*	–0.41	0.05/0.01/0.04
Si-C3				0.35			0.00/0.00/0.00
Si-C4				0.26			0.02/0.00/0.02
Si-C5				0.08			0.00/0.00/0.00
LV(Si)	0.35		p				
LV(Si)	0.31		sp$^{18.89}$				
LP(Fe)	1.87		d				
LP(Fe)	1.75		d				
LP(Fe)	1.74		d				
LP(Si)	1.95		sp$^{0.14}$				
LP(C2)	1.05		p				
σ*(Fe–Si)	0.37	23.4 (Fe) 76.6 (Si)	sd$^{3.44}$ (Fe) sp$^{13.28}$ (Si)				

[a]: occ.: occupancy, pol: polarization, hyb.: hybridization, WBI: Wiberg bond index. [b]: Partial charges obtained by natural population analysis (NPA). [c]: tot.: total, cov.: covalent.

Table S12: Selected results of the second order perturbation theory analysis of the Fock matrix in the NBO basis of [Cp*(CO)$_2$FeSi(η^3-Cp*)]$_{calc}$.

Donor orbital	Acceptor orbital	Interaction energy [kcal mol^{-1}]
σ(Fe–Si)	σ*(Fe–Si)	55.6
π(C3-C4)	LV(Si)	61.0
σ(C3-C4)	LV(Si)	6.5
LP(C2)	π*(C3-C4)	78.5
LP(C2)	π*(C5-C1)	53.8